Spring 5-2020

Electrophysiological characterization of the inhibitory effects of 2-amino-4-bis (aryloxy benzyl) amino butanoic acids on alanine serine cysteine transporter 2 and sodium coupled neutral amino acid transporter 2

Paul Serguei Zakrepine
Binghamton University--SUNY, pzakrep1@binghamton.edu

ELECTROPHYSIOLOGICAL CHARACTERIZATION OF THE INHIBITORY EFFECTS OF 2-AMINO-4-BIS (ARYLOXY BENZYL) AMINO BUTANOIC ACIDS ON ALANINE SERINE CYSTEINE TRANSPORTER 2 AND SODIUM COUPLED NEUTRAL AMINO ACID TRANSPORTER 2.

BY

PAUL SERGUEI ZAKREPINE

BS in Biochemistry, State University of New York at Binghamton, 2020

HONORS THESIS

Submitted for research in the field of Biochemistry in the Undergraduate Bachelor of Science program at Binghamton University, State University of New York, 2020

Accepted for outstanding research in the field of Biochemistry in the Undergraduate Biological Sciences Program at Binghamton University, State University of New York, May 2020

Professor Christof Grewer, Faculty Advisor, Department of Chemistry, Binghamton University

Professor Susan Bane, Chair, Department of Chemistry, Binghamton University

Professor Robert VanBuskirk, Member, Department of Biological Sciences, Binghamton University

Abstract

Alanine Serine Cysteine Transporter 2 (ASCT2) is a member of the solute carrier 1A (SLC1A) family of transport proteins. It is a Na^+ dependent, obligatory neutral amino acid exchanger with the capability to transport glutamine and it is a primary glutamine transport protein in cancer cells. This glutamine transport capability confers an important physiological role for ASCT2 in the maintenance of intracellular amino acid pools for various metabolic and cell signaling pathways. Because of this, ASCT2 is found to be overexpressed in many cancers, which rely heavily on glutamine as an essential nutrient for cell survival and growth. A wealth of research demonstrating overexpression of ASCT2 in cancer cells has made it a target for the synthesis of specific pharmacological inhibitors with the goal of killing cancer cells by glutamine starvation. A recent class of compounds known as AABA (2-amino-4-bis (aryloxy benzyl) amino butanoic acids) have been reported to have high binding affinity to ASCT2 and inhibit its function. The specificity of these inhibitors was contested and it was found that two of the most potent compounds synthesized, Compound 12 and V-9302, do not bind to ASCT2, but instead inhibit the function of two membrane transporters of different families, SNAT2 and LAT1. However, electrophysiological characterization of these inhibitors to either ASCT2 or SNAT2 has not been reported in the literature. Electrophysiological characterization has several benefits, including its high time resolution and accurate current recordings of membrane transport processes, that make it useful for measuring kinetic parameters associated with substrate or inhibitor binding such as K_i values. Herein we present the first electrophysiological characterization of several AABA compounds towards ASCT2 and SNAT2 by whole cell patch clamp current recordings and illustrate that each tested compound show variability in their inhibition toward ASCT2 or SNAT2, with some compounds presenting as more potent inhibitors

of ASCT2 while others as more potent inhibitors of SNAT2. However, each compound was shown to bind to and inhibit the protein in some manner, some, albeit, at much higher concentrations than reported in the literature. Notably some of the tested compounds are the first known blockers of SNAT2 transport.

Acknowledgements

I would like to thank the following individuals:

- **Dr. Christof Grewer** for accepting me into his lab and entrusting me to carry out such a big project. In addition to being a great teacher, your support for my endeavors and guidance throughout my undergraduate experience has been immense and I really appreciate all you've done for me. I'm thankful for the years I spent in your lab and it has been an absolute pleasure.

- **Elias Ndaru** for basically teaching me most of what I know about organic synthesis and patch clamping. With your patience and expertise, I've learned more than I could have ever imagined in these past 2 years. You have been a better teacher than I could have ever asked for and I'm happy to call you a friend. It may seem strange, but some of my most fond memories in undergrad are late nights spent in the lab doing synthesis or patch clamping with you and laughing about our suffering. Cheers and thank you for everything, Capricorn.

- **Laura Zielewicz** for helping me out with patch clamping when I was having those bad days. Trust me, it may not seem like it but the times when you would help me get cells when I was struggling were an immense help and I really appreciate it.

- **Dr. Susan Bane** for sitting on the committee and being a fantastic guide through this whole process by answering my innumerable questions and for being a great teacher in Bio Organic, I absolutely loved the class and it ended up being one of the best ones I've taken here.

- **Dr. Robert VanBuskirk** for sitting on the committee and accepting me as a teaching assistant for Cell Biology. I had a blast TA'ing for that class and I am thankful for your support in this and my future endeavors.

- **Christopher Coble** for helping me synthesize compound 19 and giving me the opportunity to teach the skills that I was lucky enough to have learned.

Table of Contents

List of Figures and Tables ix
Chapter 1: Introduction 1
1.1: Metabolism in Cancer Cells: A Brief Overview 1
1.2: ASCT2: Alanine Serine Cysteine Transporter 2: Background 3
1.3: ASCT2: Crystal Structures, Binding Site Characterization, and Transport Mechanism 3
1.4: SNAT2: Sodium Coupled Neutral Amino Acid Transporter 2 6
1.5: AABA Inhibitors: ASCT2 Specific or Off-Target Effects? 7
1.6: The Patch Clamp: Set-up, Important Principles, and its Application to the Characterization of ASCT2 and SNAT2 Inhibitors 11
C**hapter 2: Methods and Materials** 15
2.1: General Procedure for Synthesis and Associated Mechanisms of AABA Compounds 15
2.1.1: Coupling 15
2.1.2: Aqueous Workup 17
2.1.3: Purification via Flash Silica Gel Column Chromatography 18
2.1.4: Deprotection with 4M HCl/dioxane Under Reflux 18
2.2: Cell Culture and Transfection 21
2.3: Whole Cell Patch Clamp Recording 22
2.3.1: Preparation of Solutions for Testing 23
2.3.2. Whole-Cell Current Recording and Solution Exchange 24
C**hapter 3: Results** 26
3.1: Synthesis 26
3.2: NMR Spectra 27
3.2.1: Compound 6 Protected 28
3.2.2: Compound 12 Protected 29
3.2.3: Compound 12 Deprotected 31
3.2.4: Compound 19 Protected 32
3.2.5: Compound 19s: Protected 34
3.3: Patch Clamp Data: Dose Response Curves and Current Traces 36
3.3.1: Compound 6 37
3.3.2: Compound 12 39
3.3.3: Compound 19 40

3.3.4: Compound 19s 41
3.3.5: V-9302 42
Chapter 4: Discussion 45
Chapter 5: Conclusion 50
Bibliography 51

List of Figures and Tables

Figure 1: Schematic diagram of glutaminolysis as it occurs in the mitochondria 2
Figure 2: Proposed one gate elevator mechanism for substrate translocation in ASCT2..... 5
Figure 3: Ion exchange mechanism of ASCT2 that occurs during amino acid exchange 5
Figure 4: Electrogenic transport in SNAT2. 7
Figure 5: AABA based compounds tested by electrophysiology 10
Figure 6: Diagram of patch clamp set-up. 11
Figure 7: Hill plot equation using current measurements to determine K_i values. 13
Figure 8: Modified Hill plot equation 14
Figure 9: General synthetic scheme for the synthesis of AABA compounds 16
Figure 10: Reductive amination mechanism for the synthesis of AABA compounds.. 16
Figure 11: TLC analysis of compound 19 with labeled components for reference. 17
Figure 12: General synthetic scheme for the deprotection of AABA compounds. 19
Figure 13: Example TLC analysis of deprotected compound 6 after precipitation 19
Figure 14: Reflux apparatus for deprotection in HCl/dioxane for AABA compounds 20
Figure 15: Patch clamp set-up with appropriate parts of the apparatus labelled. 23
Figure 16: Stopped flow solution dispensing system. 24
Figure 17: Position of the cell near the solution exchange 25
Figure 18: Current at various pipette positions. 25
Figure 19: Compound 6 protected ^{1}H NMR 28
Figure 20: Compound 12 protected ^{1}H NMR 29
Figure 21: Compound 12 protected ^{13}C NMR. 30
Figure 22: Compound 12 deprotected ^{1}H NMR. 31
Figure 23: Compound 19 protected ^{1}H NMR 32
Figure 24: Compound 19 protected ^{13}C NMR 33
Figure 25: Compound 19s protected ^{1}H NMR. 34
Figure 26: Compound 19s protected ^{13}C NMR. 35
Figure 27: Compound 6 dose response curves and current recording traces 37
Figure 28: Compound 12 dose response curves and current recording traces 39
Figure 29: Compound 19 dose response curves and current recording traces 40
Figure 30: Compound 19s current recording traces 41
Figure 31: V-9302 dose response curves and current recording traces 42

Table 1: Yields of protected and deprotected AABA compounds 27
Table 2: K_i values obtained for each AABA compound 44

Chapter 1: Introduction

1.1: Metabolism in Cancer Cells: A Brief Overview

Unlike normally functioning cells, cancer cells undergo a shift in metabolism. This shift includes several changes that make cancer cells distinct from normal, healthy cells. There is a preferred metabolic shift towards glycolysis, even in aerobic environments, known as the Warburg effect (Liberti, M. V, & Locasale, J. W., 2016). Additionally, there is an increase in glutamine uptake observed in cancer cells. Glutamine is the most abundant amino acid found in plasma, making it a plentiful resource for cancer cells to utilize (Souba, W. W., 1993). An important use of glutamine by cancer cells is as a catabolic substrate that can be broken down into citric acid cycle metabolites in a process known as glutaminolysis (Yang, L. et al., 2017). Glutamine is a fundamental amino acid for the proliferation, growth, and survival of cancer cells, therefore, targeting proteins that regulate glutamine uptake into cancerous cells is a field of research with high potential for future clinical applications in cancer treatments (Souba, W. W., 1993).

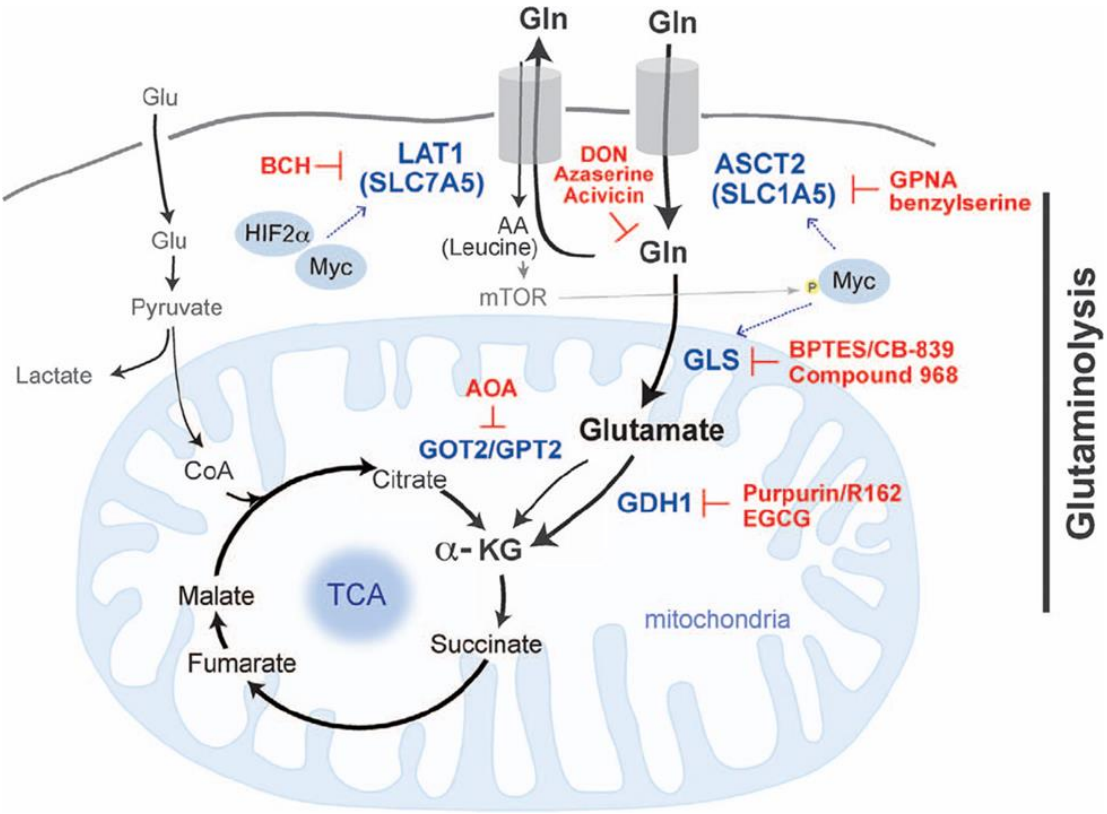

Figure 1: Schematic diagram of glutaminolysis as it occurs in the mitochondria by transport of glutamine through ASCT2 (Jin, L. et al., 2016).

As illustrated in Figure 1, glutamine is important in normal cell process such as glutaminolysis, where glutamine is broken down and fed into the citric acid cycle in the form of α-ketoglutarate. This process occurs in normal healthy cells, but it is seen in significantly higher volumes in cancer cells than in normal cells (Yang, L., Venneti, S., & Nagrath, D., 2017). This is just one of the ways that cancer cells utilize the high concentration of plasma glutamine. The other ways that glutamine is utilized include activation and sustaining cell growth signaling pathways such as mTOR (mammalian target of rapamycin), increased glucose uptake by suppression of proteins that regulate glucose uptake, and increased resistance to cell senescence and cell death (Hensley, C. T. et al., 2013).

1.2: ASCT2: Alanine Serine Cysteine Transporter 2: Background

ASCT2 is a membrane bound transport protein that belongs to the solute carrier 1A family (SLC1A) of membrane transport proteins and is an important protein in the regulation of the concentrations of extracellular and intracellular amino acid pools. It is unique in that it is the only member of this family with the ability to transport glutamine, making it an important component for glutamine metabolism (Napoli, E et al., 2018). Because of this, ASCT2 plays a significant role in the growth and survival of cancer cells, which rely more heavily on glutamine than normal cells, and it is highly upregulated with much higher expression than normal cells. These include cancers such as breast cancer and prostate cancer, making it a target of interest for the synthesis of pharmacological inhibitors (Wang, Q et al., 2015; Van Geldermalsen, M et al., 2016). Because of their potential as effective targets for the treatment of various cancers, the synthesis and testing of ASCT2 inhibitors has become a rapidly growing field of research.

1.3: ASCT2: Crystal Structures, Binding Site Characterization, and Transport Mechanism

ASCT2 or SLC1A5 is an electroneutral amino acid exchanger, in which amino acid transport is coupled to the co-transport of Na^+ ions but is not driven by this transport through a secondary active transport mechanism (Bröer A. et al., 2000). The electroneutrality of ASCT2 means that it does not produce a change in the membrane potential of the cell. Unlike the excitatory amino acid transporters (EAAT's) and the archaeal prokaryotic transporters, Glt_{Ph} and Glt_{Tk}, other members of the SLC1A family of glutamate transporters, which are electrogenic and undergo concentrative acid amino acid transport (Divito, C. B., & Underhill, S. M., 2014; Ji, Y et al., 2016; Scopelliti, A. J. et al., 2018). However, structural characterization of the members of this family has allowed for the development of homology models used to further understand the

structural basis of neutral amino acid exchange in the SLC1A family and to elucidate important substrate binding residues in ASCT2 by sequence alignments and reverse mutagenesis to more fully understand ASCT2's specificity to glutamine (Scopelliti, A. J. et al., 2018). Furthermore, ASCT2 follows an antiporter mechanism in which Na^+ ions and a neutral amino acid from the extracellular portion of the cell membrane are exchanged for a neutral amino acid on the intracellular side (Utsunomiya-Tate et al., 1996; Kanai & Hediger, 2004). In addition, ASCT2, along with the rest of the proteins in the SLC1A family, has a thermodynamically uncoupled leak anion conductance, in which ASCT2 allows anions like SCN^- to flow across the cell membrane through it (Broer A. et al., 2000; Grewer, C., & Grabsch, E., 2004). This leak anion conductance is the basis for electrophysiological characterization of ASCT2 because in the presence of substrates such as alanine, at 0 mV, inwardly directed currents are observed, while in the presence of inhibitors, apparent outwardly directed currents are observed as an indication of the inhibition of the leak anion conductance (Grewer, C., & Grabsch, E., 2004). The direction of the currents depends on the experimental buffer conditions used, but the trend is still consistent. Additionally, recent crystal structures have revealed that it is a homotrimeric protein and its three identical monomers each contain a scaffold and transport domain (Yu, X. et al., 2019). In recent years, an inward open crystal structure of ASCT2 has elucidated a possible mechanism for ASCT2 substrate transport by a one gate elevator mechanism in which the specific hairpin loop, HP2, acts as the gate on both the extracellular and intracellular substrate binding domains of the protein. The substrate is translocated through the cellular membrane through conformational changes of the transport domains of the protein, while the scaffold domains remain stationary (Garaeva, A. A. et al., 2019; Yu, X. et al., 2019). A recent outward open cryo-EM structure of ASCT2, in combination with the inward facing state, has elucidated more information about

specific loops and structures within the protein that are critical to the transport mechanism of ASCT2 (Yu, X. et al., 2019). The recently proposed one gate elevator mechanism is illustrated in Figure 2, in addition to the electroneutral exchange mechanism of ASCT2 in Figure 3.

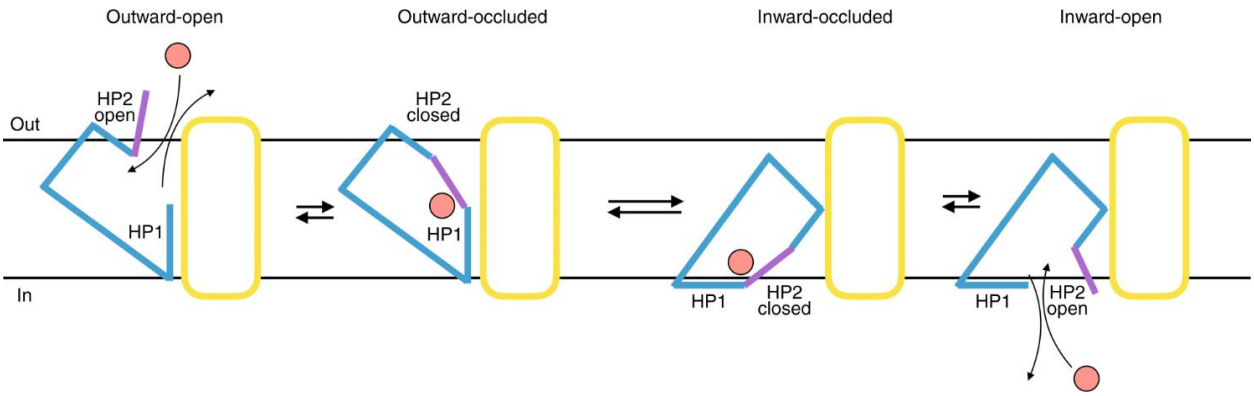

Figure 2: Proposed one gate elevator mechanism for substrate translocation in ASCT2. In the Na^+ dependent process, the substrate binds to the substrate binding site in the transport domain in the outward open conformation. After closing of HP2, conformational changes allow for exchange of substrate to the intracellular side of the cell. Release of the extracellular substrate in the intracellular site allows for binding of an intracellular amino acid (Garaeva, A. A. et al., 2019).

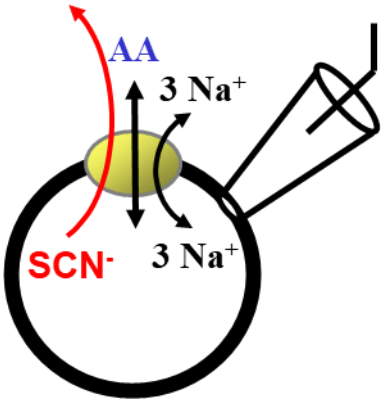

Figure 3: Ion exchange mechanism of ASCT2 that occurs during amino acid exchange. In addition, the direction of the thermodynamically uncoupled anion conductance is illustrated as well. This figure was provided by Elias Ndaru.

Amino acid exchange in normal physiological conditions for ASCT2 is electroneutral, as illustrated by the stoichiometry of Na^+ exchange. The uncoupled anion conductance is what causes changes in potential across the membrane and produces currents for analysis and calculation of kinetic constants. Interestingly, chloride anions are not permeable to the anion conducting pore and the physiological significance of this pore is not known, as SCN^- anions are not present in the extracellular or intracellular medium of cells. However, the significance of this anion conductance comes from the ability of researchers to use electrophysiology to characterize kinetic constants for inhibitors and substrates using currents produced by anion conductance in a dose dependent manner (Broer A. et al., 2000; Grewer, C., & Grabsch, E., 2004).

1.4: SNAT2: Sodium Coupled Neutral Amino Acid Transporter 2

SNAT2 is an electrogenic neutral amino acid transporter, that is coupled to intracellular transport of one Na^+ ion through a symporter mechanism (Zhang, Z. et al., 2011). SNAT2 belongs to the solute carrier 38 transporter family, SLC38, which is involved with the unidirectional transport of neutral amino acids into the cell, including glutamine. SNAT2 falls mainly under the category of system A activity, which is associated with transport of short chain aliphatic amino acids specifically into the cell, and therefore regulation of intracellular amino acid pools (Bröer, S., 2014).

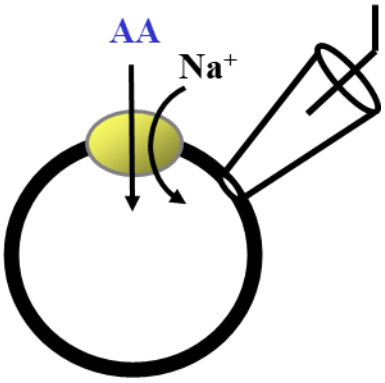

Figure 4: Electrogenic co-transport of one Na^+ ion for each amino acid transported via SNAT2. This figure was provided by Elias Ndaru.

As illustrated in Figure 4, amino acid transport by SNAT2 is an electrogenic process (Zhang, Z. et al., 2011). Additionally, it plays an important role in the osmotic regulation of cell volume in hypertonic conditions (Franchi-Gazzola, R. et al., 2004). Furthermore, and an important reason for it as a target of interest, is the upregulation of SNAT2 in conditions of amino acid starvation (Hoffmann, T. M. et al., 2018). Upregulation of SNAT2 in ASCT2 knockdown conditions, and therefore amino acid starvation conditions, has been shown to be a rescue response in cancer cells, indicating that it plays an important role in maintaining glutamine uptake in cancer cells and therefore a target for the synthesis of pharmacological inhibitors (Bröer, A., et al., 2016).

1.5: AABA inhibitors: ASCT2 Specific or Off-Target Effects?

Previous inhibitors of ASCT2 have been reported in the literature, such as L -γ- glutamyl-p-nitroanilide (GPNA). However, GPNA has a poor binding affinity to ASCT2 and has been demonstrated to be nonspecific in its inhibition (Esslinger, C. S. et al., 2005; Corti, A. et al., 2019). Additionally, other compounds based on sulfonamide and sulfonic acid ester scaffolds have been characterized by electrophysiological methods and have been reported as inhibitors for

ASCT2 with K_i values as low as 8 ± 4 μM (Ndaru, E., et al., 2019). Other studies have also reported benzyl proline derivatives as effective ASCT2 inhibitors using electrophysiological characterization, with the lowest reported K_i value of 3 ± 2 μM for a biphenyl benzyl proline compound (Singh, K. et al., 2017). Recent compounds in the class of 2-amino-4-bis (aryloxy benzyl) amino butanoic acids (AABA) have been purported to be specific inhibitors of ASCT2 with IC_{50} values in the range of 1-10 μM for the most potent inhibitors of human ASCT2 (hASCT2) and rat ASCT2 (rASCT2) (Schulte, M. L. et al., 2016). IC_{50} and K_i are two ways to characterize inhibitor binding affinity in enzyme-substrate complexes, but it can be applied to inhibitor binding of transport proteins as well. IC_{50} values differ from K_i values because K_i values are a constant value for a specific inhibitory compound while IC_{50} values can vary depending on the experimental assay used and are the concentration of inhibitor needed to reduce enzymatic activity by one half the maximum in the specific conditions. In enzyme-inhibitor assays, the IC_{50} value will change with changing substrate concentrations at constant inhibitor concentrations while the K_i value for the inhibitor will remain constant. K_i values will always be lower than IC_{50} values, as they essentially represent the intrinsic inhibitor binding affinity (Burlingham, B. T., & Widlanski, T. S., 2003). This study characterized the IC_{50} values for a library of AABA compounds using a ^3H labelled glutamine uptake assay with increasing inhibitor concentrations and concluded that the inhibition constants obtained were from inhibition specific to ASCT2 in both HEK293 (human embryonic kidney cell line 293) and C6 (rat glial tumor cells) (Schulte, M. L. et al., 2016). In addition, researchers from this group synthesized a novel compound from the AABA scaffold known as V-9302, and they demonstrated in a variety of cancer cell lines that this compound inhibits viability, growth, and survival of tumor cells *in vitro* and *in vivo* in mice by the inhibition of glutamine uptake in

ASCT2 (Schulte, M. L. et al., 2018). However, recent experimental assays have shown that the AABA inhibitors, Compound 12 and V-9302 may not be specific to ASCT2, but instead, the possibility was proposed that they are inhibitors of the membrane proteins SNAT2 (sodium dependent neutral amino acid transporter) and LAT1 (large neutral amino acid transporter), which are also upregulated and critical to cancer metabolism (Bröer, A. et al., 2018). These experiments showed that inhibition of glutamine uptake in the presence of AABA inhibitors with cells containing ASCT2 and cells with ASCT2 deletions showed identical inhibition. Additionally, through glutamine uptake experiments, these researchers discovered a large inhibition of system A activity in cells without ASCT2, that expressed SNAT2, indicative that these compounds inhibit SNAT2 and not ASCT2. Additionally, it was discovered that AABA compounds inhibit LAT1 activity as well (Bröer, A. et al., 2018). LAT1 is another relevant protein that is an antiporter of essential amino acids and plays an important role in cancer metabolism and import of leucine for use in cell signaling pathways (Scalise, M., et al., 2018). In addition, there have been no tests using electrophysiological methods to characterize the binding affinity of AABA compounds to ASCT2 and SNAT2. Here, we use electrophysiological characterization to determine the K_i values for four AABA compounds reported in Schulte et al. (2016 & 2018), in addition to a derivative with a single side chain. Two of these compounds, compound 12 and V-9302, were tested by Bröer, A. et al. (2018) and were determined to have off target, nonspecific effects, in the inhibition of glutamine uptake by ASCT2. The other two inhibitors, compound 6 and compound 19, have not been tested by our group or others. The literature reported IC_{50} values and the structure of these compounds is illustrated in Figure 5.

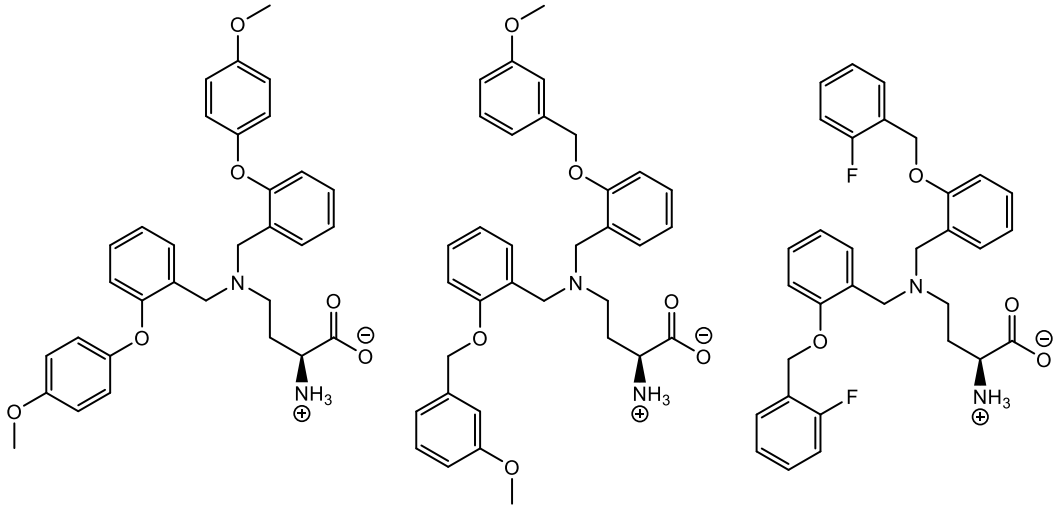

Compound 6
Proposed IC_{50} Values
hASCT2: 8.7 μM +/- 0.5 μM
rASCT2: 11.9 μM +/- 0.4 μM

Compound 12
Proposed IC_{50} Values
hASCT2: 7.2 μM +/- 0.5 μM
rASCT2: 5.1 μM +/- 1 μM

Compound 19
Proposed IC_{50}Values
hASCT2: 7.9 μM +/- 1.9 μM
rASCT2: 3.3 μM +/- 1.4 μM

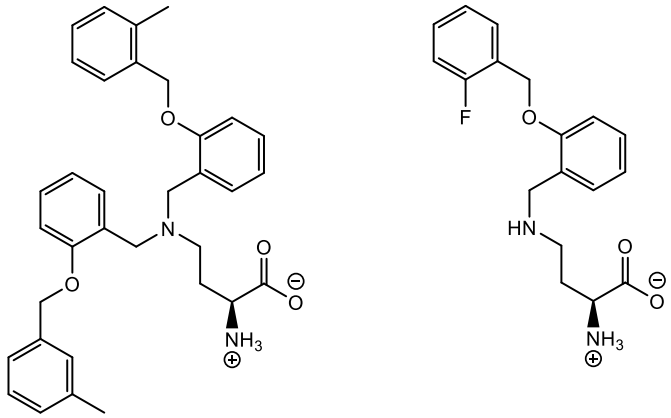

V-9302
Proposed IC_{50}Values
hASCT2: 9.6 μM
rASCT2: N/A

Compound 19 Single
Proposed IC_{50}Values
hASCT2: N/A
rASCT2: N/A

Figure 5: AABA based compounds tested by electrophysiology and their purported literature IC_{50} values (Schulte, M. L. et al., 2016 & 2018). Compound 19 single is referred to as 19s throughout the paper.

1.6: The Patch Clamp: Set-up, Important Principles, and its Application to the Characterization of ASCT2 and SNAT2 Inhibitors

Here we use electrophysiological techniques in the form of whole cell voltage clamp current recording (patch clamp) to measure transient steady state currents produced by substrate or inhibitor binding to ASCT2 and SNAT2. The patch clamp technique is useful in this context because it can be used to determine kinetic constants associated with substrate or inhibitor binding, such as K_i values. In addition, the patch clamp technique confers several advantages in this experimental characterization because of its sensitivity, high time resolution, and it does not require fluorescent or radioactively labelled substrates (Grewer, C. et al., 2013). A diagram of the current recording system used in the whole cell patch clamp set up is illustrated in Figure 6.

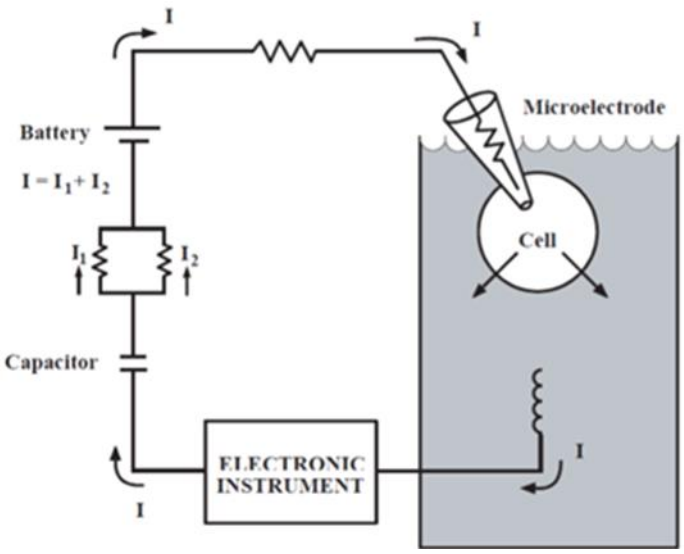

Figure 6: Currents produced by cellular process, such as ion conductance, are measured by the flow of different ions between the cell, which is buffered by an internal salt solution that is present inside the pipette, and the extracellular solution. Currents are recorded by silver microelectrodes present in both the micropipette and external solution. (Molecular Devices, 2012).

The patch clamp technique is a technique in which a micropipette filled with an internal salt solution is pressed onto a cell, and a small amount of suction is applied to break the plasma membrane. As illustrated in Figure 6, the pipette contains an Ag/AgCl microelectrode used to record these currents, in addition to one inside the extracellular buffer. By breaking the plasma membrane, the cell can enter "whole cell" recording mode, in which the pipette is in communication with the entirety of the cell cytosol, and therefore all the ASCT2 proteins being expressed within the cell membrane. A small voltage pulse can also be applied to the membrane to break it into whole cell mode (Molecular Devices, 2012). By being in communication with the entirety of the cell, the sum of all the currents produced by leak anion conductance of every expressed ASCT2 protein can be measured simultaneously. Currents are measured without changes in voltage because the voltage is clamped to a constant value by injection of an appropriate current (Grewer, C. et al., 2013). For ASCT2, the internal solution contains 130 mM NaSCN as the major ions, while the external solution contains 140 mM NaCl. In its normal resting state, ASCT2 has a natural leak anion conductance, enabling the transmembrane flow of anions down their concentration gradient (Grewer, C., & Grabsch, E., 2004). In the given experimental conditions, SCN^- flows down its concentration gradient from the intracellular to the extracellular side of the cell. This can be observed in the patch clamp set up as a more positive membrane potential when the recording enters whole cell mode. However, with substrate bound, this leak anion conductance is increased, leading to the production of inwardly directed currents. In the presence of inhibitors, this leak anion conductance is inhibited, and leads to the production of apparent "outwardly" directed currents (Grewer, C., & Grabsch, E., 2004). This apparent "outward" current is really caused by the reduction (inhibition) of the inwardly directed tonic leak anion current. By measuring these currents at a constant voltage with increasing inhibitor

concentrations, a K_i value for the specific compound for ASCT2 can be calculated based on the response from the cells via the production of currents. Alanine substrate is placed on the intracellular side of the solution for ASCT2 to keep it in its activated, outward-facing state for current recording. This is because alanine on the intracellular side leaves the extracellular binding site in a position where it is open to accept substrate (Grewer, C. et al., 2013). If values of the currents produced in increasing inhibitor concentration are plotted to saturation response and they fit a curve that resembles Michaelis-Menten like enzyme kinetics, then the Hill plot equation can be used to calculate the K_i value specific to ASCT2 for the compound. The version used to characterize inhibitor binding affinity by electrophysiology is slightly modified to use relative current values instead of the typical V/V_{max} for the y-value in Figure 7.

$$y = \frac{I_{max}\,[Inhibitor]}{[Inhibitor] + K_i}$$

Figure 7: Hill Plot equation using current measurements to determine K_i values for inhibitors. Y is equal to the current at each inhibitor concentration relative to the current produced at the highest inhibitor concentration (I/I_{max}).

To produce meaningful analyzed data, the currents for these traditional electrophysiological inhibitor experiments are normalized to 1 using the largest outward current produced. Each current is divided by the largest current value in pA at the maximum inhibitor concentration used, and then plotted against each respective inhibitor concentration to produce a dose response curve. Additionally, competitive experiments using constant alanine (ASCT2 and SNAT2 substrate) concentrations in the presence of increasing inhibitor concentrations can be used to reveal possible competitive inhibition in ASCT2 and SNAT2 by these compounds. If there is little to no inhibition of the leak anion conductance with solutions of increasing inhibitor concentration, these competitive experiments can be performed for greater insight into inhibition

of ASCT2. However, SNAT2 inhibitors can only be characterized by these competitive experiments as they only produce inwardly directed currents based on their transport mechanism. Unlike ASCT2, the internal solution for SNAT2 used is 130 mM KMes. There is a small leak anion conductance associated with substrate binding of SNAT2, however, it is very small compared to the one produced by ASCT2 and not useful for measuring currents produced by inhibitor binding (Zhang, Z., & Grewer, C., 2007). In the presence of SNAT2 inhibitors, the alanine-induced inwardly-directed transport current is reduced compared to the control with alanine alone, because inhibition decreases the amount of Na^+ ions flowing from the extracellular solution to the intracellular side, therefore decreasing the magnitude of the inwardly directed current. For these experiments, a modified version of the Hill plot equation is used. This is to account for the increase in current values in the direction of negative values towards zero, in contrast to the previously mentioned experiments, which are only concerned with increasingly positive currents. The equation used is pictured in Figure 8.

$$y = I_1 + \frac{I_2\,[Inhibitor]}{K_i + [Inhibitor]}$$

Figure 8: Equation used to calculate K_i values for inhibitors using data from alanine competition experiments, where I_1 is the current produced by alanine without inhibitor present and I_2 is the current produced by the highest inhibitor concentration in the presence of alanine. Y is equal to current produced by Inhibitor + Ala divided by the current produced by alanine without inhibitor (Ndaru, E. et al., 2019).

Each current is divided by the most negative inward current produced, which in each case should be the alanine control. This is to normalize the values to -1. The currents in these experiments were recorded at 0 mV, as we are not concerned with the voltage dependence of inhibitor and substrate binding.

Chapter 2: Methods and Materials

2.1: General Procedure for Synthesis and Associated Mechanisms of AABA Compounds

All AABA compounds were synthesized and deprotected by the same procedure, except V-9302, which was purchased from MedChem Express. Compound 19 was synthesized, purified, analyzed, and deprotected by Christopher Coble.

2.1.1: Coupling

2-amino-4-bis (aryloxy benzyl) amino butanoic acids (AABA) compounds were synthesized via a reductive amination synthetic scheme (Schulte, M. L. et al., 2016). The starting materials included each AABA compounds respective side chain in its benzaldehyde form with the remaining portion of the side chain ortho to the aldehyde position. 2,4 diamino butanoic acid was kept constant as the amine used for each synthesis and was the limiting reagent in each reaction. Compounds coupled to two identical side chains used 3 equivalents of aldehyde, while compounds coupled to a single side chain used 1.1 equivalents of aldehyde. These two components were added to a clean, oven-dried, round bottomed flask (RBF) with a magnetic stir bar. A rubber stopper was placed on the RBF and connected to N_2 flow via two needles, for inflow and outflow, to displace any air in the reaction vessel along with possible moisture, for 5-10 minutes. Dry dichloromethane (DCM) was added via a 10 mL syringe with an oven dried needle under N_2 to the reaction mixture at 0 °C. The mixture was then stirred for 10 minutes at 0 °C under N_2. The rubber stopper was then removed from the RBF and 2 equivalents of sodium triacetoxy borohydride ($NaBH(OAc)_3$) was added to the reaction mixture. The stopper was placed back on the vessel and the reaction was stirred at 0 °C for 30 more minutes under N_2, then left to stir for 24 hours at room temperature. Appearance of products was confirmed by

comparison of starting materials to the reaction mixture via silica thin layer chromatography (TLC) after 24 hours. TLC plates were analyzed under UV light at 254 nm and then stained in a solution of 0.2 % ninhydrin and 0.5% acetic acid in butanol to identify the presence of amine groups. An image of the TLC plate after reaction, a sample synthetic scheme, and the mechanism associated with the reaction are illustrated in Figure 9, 10, and 11.

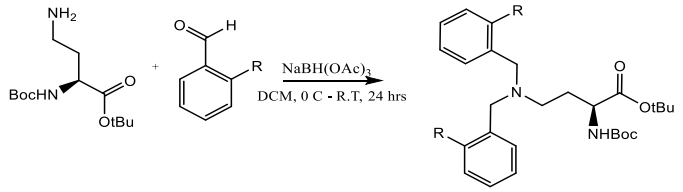

Figure 9: General synthetic scheme for the synthesis of AABA compounds (Schulte, M. L. et al., 2016).

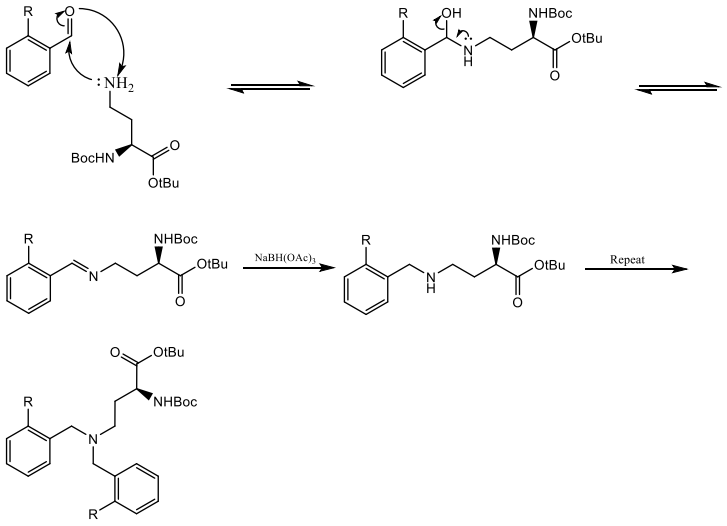

Figure 10: Reductive amination mechanism for the synthesis of AABA compounds. The reaction mechanism proceeds through an unstable imine intermediate. The addition of the reducing agent is required to shift the equilibrium in favor of the amine product. For single coupled side chains, the mechanism ends at the formation of the secondary amine. For products with two side chains, the mechanism repeats because of the presence of the additional amine hydrogen to form a tertiary amine (Abdel-Magid, A. F., & Mehrman, S. J., 2006).

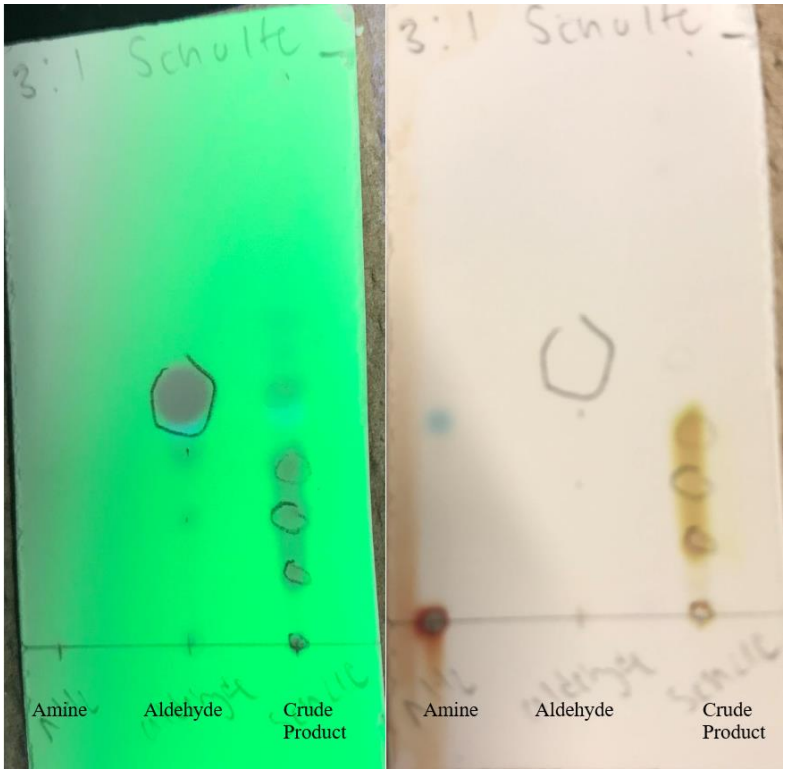

Figure 11: TLC analysis of compound 19 with labeled components for reference. There is a low concentration of the amine (limiting reagent) indicative that the reaction is near completion. The reaction components were ran on 3:1 hexane: ethyl acetate and analyzed under UV to visualize aromatic components (left). UV visible components were circled, and the plate was stained under ninhydrin (right) to indicate the presence of amines.

2.1.2: Aqueous Workup

Aqueous byproducts and waste were purified from the crude reaction mixture via a workup with distilled water. The crude mixture was rinsed three times with distilled water and the organic layer was collected in a dry Erlenmeyer flask, dried over Na_2SO_4, filtered via suction filtration, and then concentrated and dried in-vacuo.

2.1.3: Purification via Flash Silica Gel Column Chromatography

The post workup reaction mixture was then purified via flash silica gel column chromatography. Reaction mixtures were dissolved in approximately 2 mL of a 3:1 hexane: ethyl acetate solvent mixture. Glass columns were loaded with silica gel, and silica (the stationary phase) was then dissolved in hexane (the mobile phase). The dissolved reaction mixture was then pipetted into the column and topped with glass wool. Increasingly polar solvent mixtures of hexane/ethyl acetate were then added in 50 mL portions to elute the desired product. Product elution was determined using TLC and UV light. Di-coupled compounds typically eluted at 25% ethyl acetate: hexane while single coupled compounds eluted at approximately 35% ethyl acetate: hexane due to their increased polarity. Pure fractions were collected and analyzed using 400 MHz ^{1}H NMR and 101 MHz ^{13}C NMR spectroscopy. Other spectroscopic methods such as correlation spectroscopy (COSY) and nuclear overhauser effect spectroscopy (NOESY) were used for further analysis of each compound. Compounds were dissolved in deuterated chloroform ($CDCl_3$) for NMR analysis.

2.1.4: Deprotection with 4M HCl/dioxane Under Reflux

Compounds were dried for at least 24 hours in-vacuo. Boc and tertbutyl protection groups were then deprotected with 4M HCl in dioxane under reflux at 55 °C to yield analytically pure chloride salts in high yield. Purified compounds were dried for at least 24 hours under high vacuum in a 10 mL RBF. Reflux apparatus was assembled as shown in Figure 14 while N_2 gas was flowing. 4M HCl/dioxane (72 eq.) was added under N_2 gas and the mixture was left to stir under reflux for 24 hours. Excess HCl/dioxane reagent was removed in vacuo and the oily residue was dissolved in DCM, then the chloride salt was precipitated by the addition of chilled

hexane. The presence of product was confirmed via TLC and then ^{1}H and ^{13}C NMR analysis. The synthetic scheme for this deprotection, an image of the reflux apparatus, and TLC plate is illustrated in Figure 12, 13, and 14.

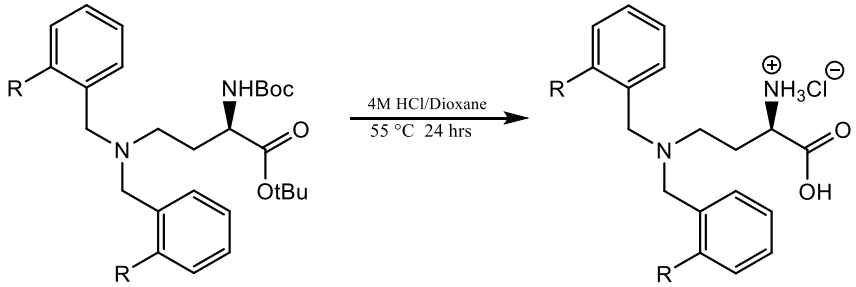

Figure 12: General synthetic scheme for the deprotection of AABA compounds (Schulte, M. et al., 2016).

Figure 13: Example TLC analysis of deprotected compound 6 after precipitation. Product was dissolved in DCM for this analysis and run in 10% methanol in DCM solvent, then stained in ninhydrin to yield the TLC plate on the right. Each spot is the same deprotected product.

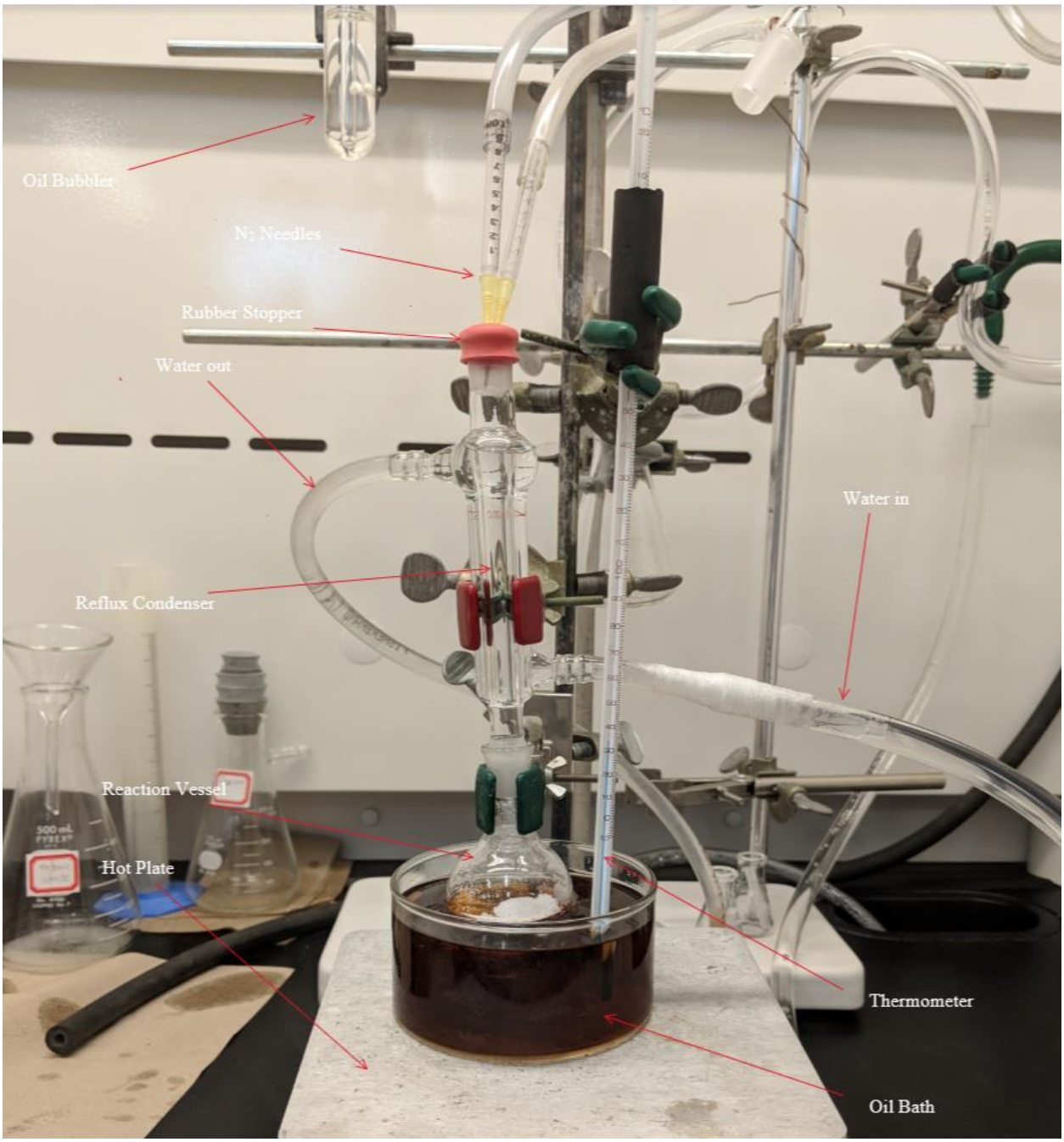

Figure 14: Reflux apparatus for deprotection in HCl/dioxane for AABA compounds with labelled components. The reflux condenser and cold-water flow in/out is necessary to re-condense any portion of the reaction mixture that evaporates at the temperatures involved. N_2 gas flows at a slow rate to displace any moisture in the reaction atmosphere, in addition to preventing the buildup of too much vapor pressure.

2.2: Cell Culture and Transfection

Rat ASCT2 (rASCT2), human ASCT2 (hASCT2), rat SNAT2 (rSNAT2) and yellow fluorescent protein (YFP) cDNA's were used to transiently co-transfect human embryonic kidney 293 (HEK293) cells using POLYPLUS Jet-prime transfection reagent. Transfection is the process of introducing a desired DNA sequence of interest into a cell with the goal of expressing the protein coded for by this sequence (Goedhart, J., et al., 2011). The DNA transfection mixture consisted of 100 μL of transfection buffer, 2 μL of transfection reagent, 0.5 μg of YFP and 0.5 μg of the respective transporter DNA and the solution was vortexed for 10 seconds.

HEK293 cells were cultured in Dulbecco's modified eagle medium (DMEM), supplemented with 10% fetal bovine serum (FBS), 2 mM glutamine, and essential amino acid mix. Cell cultures were kept in a humidified CO_2 incubator at 10% CO_2. To passage confluent HEK293 cells, old medium was removed by vacuum suction. Cells in culture flasks were then washed with phosphate buffered saline (PBS Buffer) and then underwent trypsinization using ~ 1 mL of 1% trypsin. Approximately 2 mL of fresh, sterile filtered DMEM was added to the cells. Cells were broken apart by trituration. Depending on the concentration of cells, 2-4 drops were added to a sterile plastic culture dish containing DMEM. The culture dish contained three sterile, autoclaved 12 mm glass cell culture plates coated with 0.01% poly-L-lysine in PBS to help cells attach to the surface of these dishes. Subsequently, the DNA transfection mixture was added to the plastic culture dish and the cells were placed in a 37 °C CO_2 incubator between 24-28 hours before patch clamp experiments were conducted on the cells.

2.3: Whole Cell Patch Clamp Recording

Inhibitor affinity was measured in the whole cell configuration (see paragraph below) using a patch clamp set up. Currents were recorded with an EPC7 patch clamp amplifier from ALA Scientific ® using pClamp 6 data acquisition software. Current values were determined using Clampfit and analyzed in Microsoft Excel. Data was plotted in Origin lab to formulate dose response curves and current traces for ASCT2 and SNAT2. For cells transfected with ASCT2 DNA, the external buffer was 140 mM NaCl, 2 mM $MgCl_2$, 2 mM $CaCl_2$, and 10 mM HEPES at pH 7.40, while the internal micropipette buffer used was 130 mM NaSCN, 2 mM $MgCl_2$, 10 mM EGTA, 10 mM alanine, and 10 mM HEPES at pH 7.40. For SNAT2 transfected cells, the external buffer was the same as ASCT2, while the internal buffer contained 130 mM KMes and 2 mM Mg $(Gluconate)_2$. Micropipettes were fabricated using the model P-97 Flaming/Brown micropipette puller from Sutter Instrument Co. Glass micropipettes were filled with internal buffer solution and had seal resistances between 3 and 5 MΩ. Internal salt bridges were filled with external buffer and steady state currents were recorded at 0 mV using the set up pictured below. Silver electrodes were previously soaked in bleach to generate an AgCl coating and were used as the microelectrodes. The setup is pictured in Figure 15.

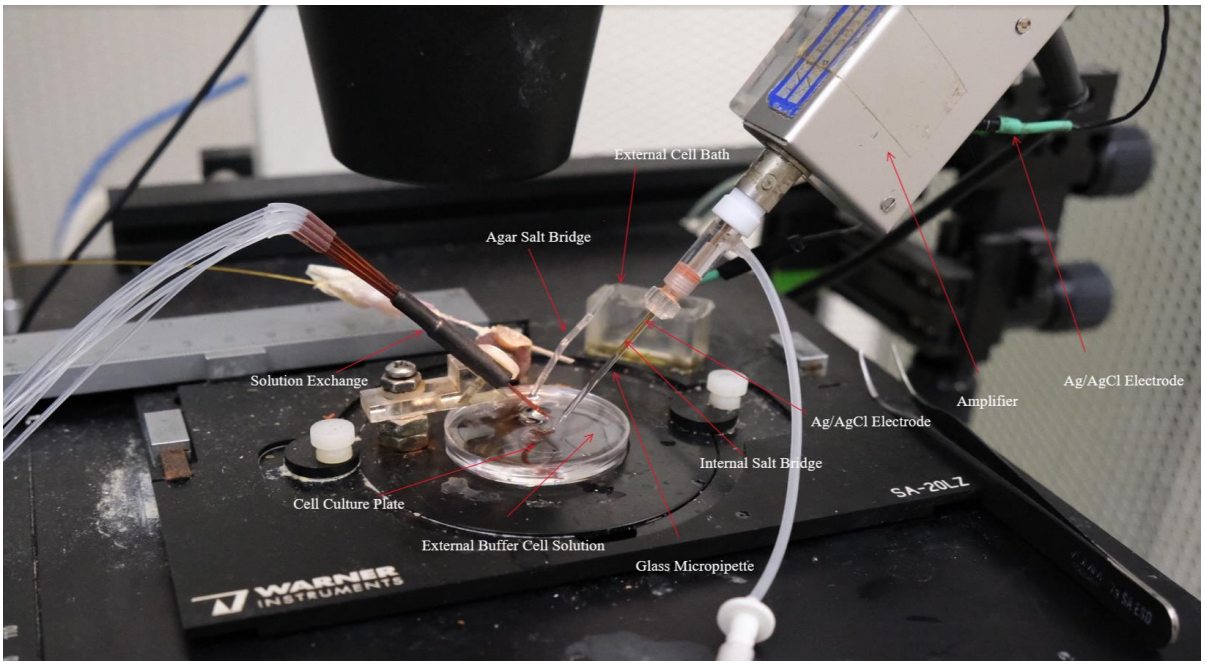

Figure 15: Patch Clamp Set-up with appropriate parts of the apparatus labelled.

2.3.1: Preparation of Solutions for Testing.

20 mM inhibitor stock solutions were prepared using deprotected chloride salts of the AABA compounds dissolved in the appropriate volume of dimethyl sulfoxide (DMSO). Inhibitor solutions were prepared using increasing volumes of DMSO stock solution dissolved in 140 mM NaCl external buffer. For competitive inhibition experiments, solutions were prepared with a constant alanine concentration using a 100 mM alanine stock solution. All solutions prepared and used for testing in this experiment contained ≤ 2% DMSO. Controls only containing buffer and DMSO were previously performed and did not show substantial effects on current recordings at concentrations up to 3% DMSO (Ndaru, E. et al., 2019). Due to solubility issues, the most concentrated inhibitor solution used was 400 μM. The placement of these inhibitor solutions in the patch clamp set up is pictured in Figure 16.

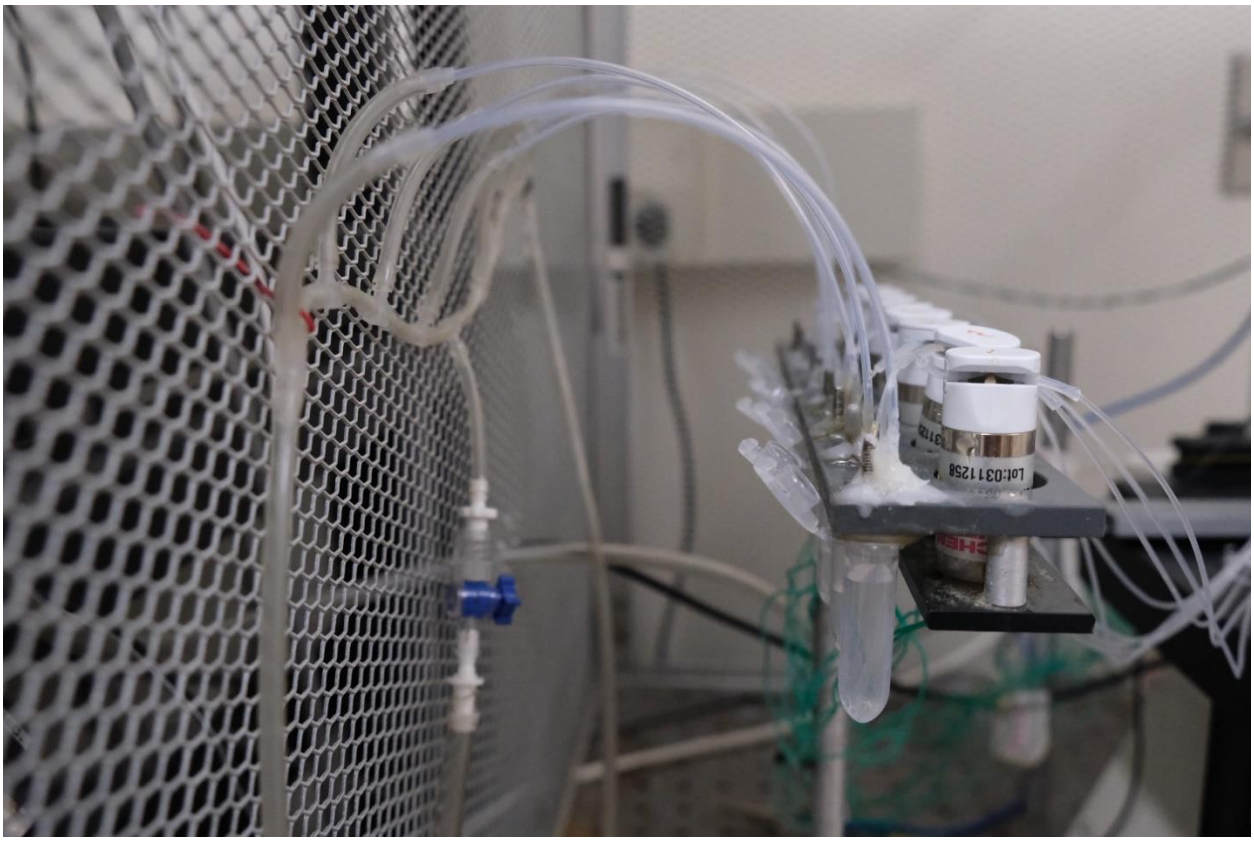

Figure 16: Stopped flow solution dispensing system with 8 Eppendorf tubes containing solution. The first tube contains external buffer for washing the cell and the second tube contains an alanine control. Tubes 3 – 8 contain increasing inhibitor concentrations.

2.3.2. Whole-Cell Current Recording and Solution Exchange

To choose a cell expressing the desired DNA, fluorescence is observed using a UV lamp. Typically, increased fluorescence from co-expressed YFP correlates with increased expression of the desired transport protein and therefore larger currents. The current recording electrode is controlled by a micromanipulator, which is used to move the electrode tip into the vicinity of the cell. Once the pipette tip gently touches the cell surface, a seal between pipette tip and membrane of at least 100 MΩ is achieved, and a small amount of suction is applied to break the cell membrane under the patch pipette. If at this point, the pipette is not in communication with the

entire cell, also known as whole cell mode, a small voltage can be applied to fully break the membrane under the patch pipette. Once whole-cell configuration is achieved, the cell is gently lifted and then placed in front of the solution exchange tube, as shown in Figure 17. In addition, changes in current in response to a probe square wave voltage pulse are demonstrated in Figure 18 along each step of the process of making the seal and achieving whole-cell configuration.

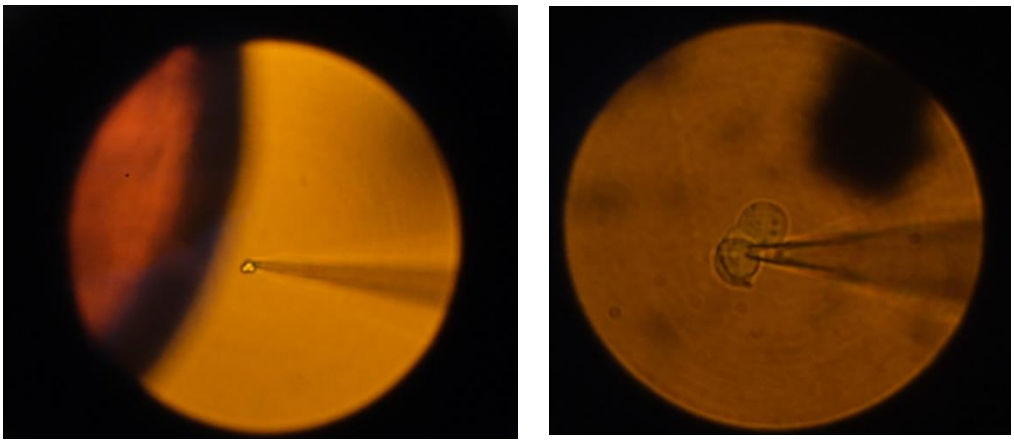

Figure 17: Position of the cell near the solution exchange (left) and high magnification view of a pipette tip touching a cell (right).

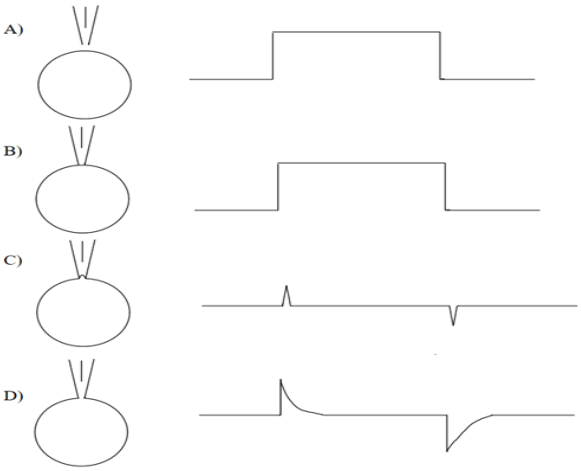

Figure 18: The appearance of current when the pipette is immersed in buffer solution (A), when the pipette touches the cell (B), when a small portion of the plasma membrane is sucked into the pipette tip (C), and whole cell mode (D).

Chapter 3: Results

3.1: Synthesis

Compounds were synthesized in analytically pure yields using reductive amination according to the synthetic scheme provided by Schulte et al. (2016). Overall, no difficulties were encountered during the initial coupling, aqueous workup, and purification by column chromatography. Both di-coupled products and suspected mono-coupled products appeared on TLC, however, syntheses focusing on the di-coupled products typically had very little of these side products and were easily purified by column chromatography. Yields of the coupled products were similar, and in some cases higher compared to the reported literature values (52-75%), except for compound 12, which had a yield of 35% deprotected compound (Schulte, M., et al., 2016). However, difficulties in the synthesis for each compound mainly came with the deprotection step. Precipitation of the product into a salt came with difficulties during filtration, as the compound would turn into an oil if left on the suction filter for a short period of time. Methods were needed to improve the filtration, so each compound was dissolved in a very small volume of DCM (< 1 mL), precipitated using ~ 3 mL of chilled hexane, and then centrifuged in a 20 mL glass vial at 9000 rpm for ~ 3 minutes. Approximately 3-5 mL of hexane was added, the solution was placed in a sonicator for 10 minutes, and then was centrifuged again. This procedure was repeated 2 more times. However, while TLC analysis showed a large abundance of the deprotected product for most compounds, compound 6 and 12 exhibited a very small spot with higher Rf value than the product that was fluorescent and stained in ninhydrin. It was suspected that this was partially deprotected product and it could not be removed regardless of the number of rinses. Mono-coupled compound 19s poorly precipitated in DCM and hexane as it was much more soluble than the di-coupled compounds, so it was left as an oil, but TLC analysis

only showed one product. All compounds were dried in vacuo for at least 48 hours before testing. Deprotected compounds were used without further purification, including those with the small contamination. The yields for the protected and deprotected compounds are listed in Table 1.

Table 1: Yields of protected AABA compounds after column chromatography and after HCl/dioxane Deprotection.

Compound (#)	Protected Yield (%)	Post-Deprotection Yield (%)
6	73	89
12	60	35
19	84	72
19s	62	92

3.2: NMR Spectra

Synthesis of pure protected compounds was confirmed by ^{1}H and ^{13}C NMR spectroscopy. Only the NMR spectra of some deprotected compounds are pictured due to problems with peak resolutions. All peaks for each compound are reported in the figure captions in Figures 19-26.

3.2.1: Compound 6 Protected

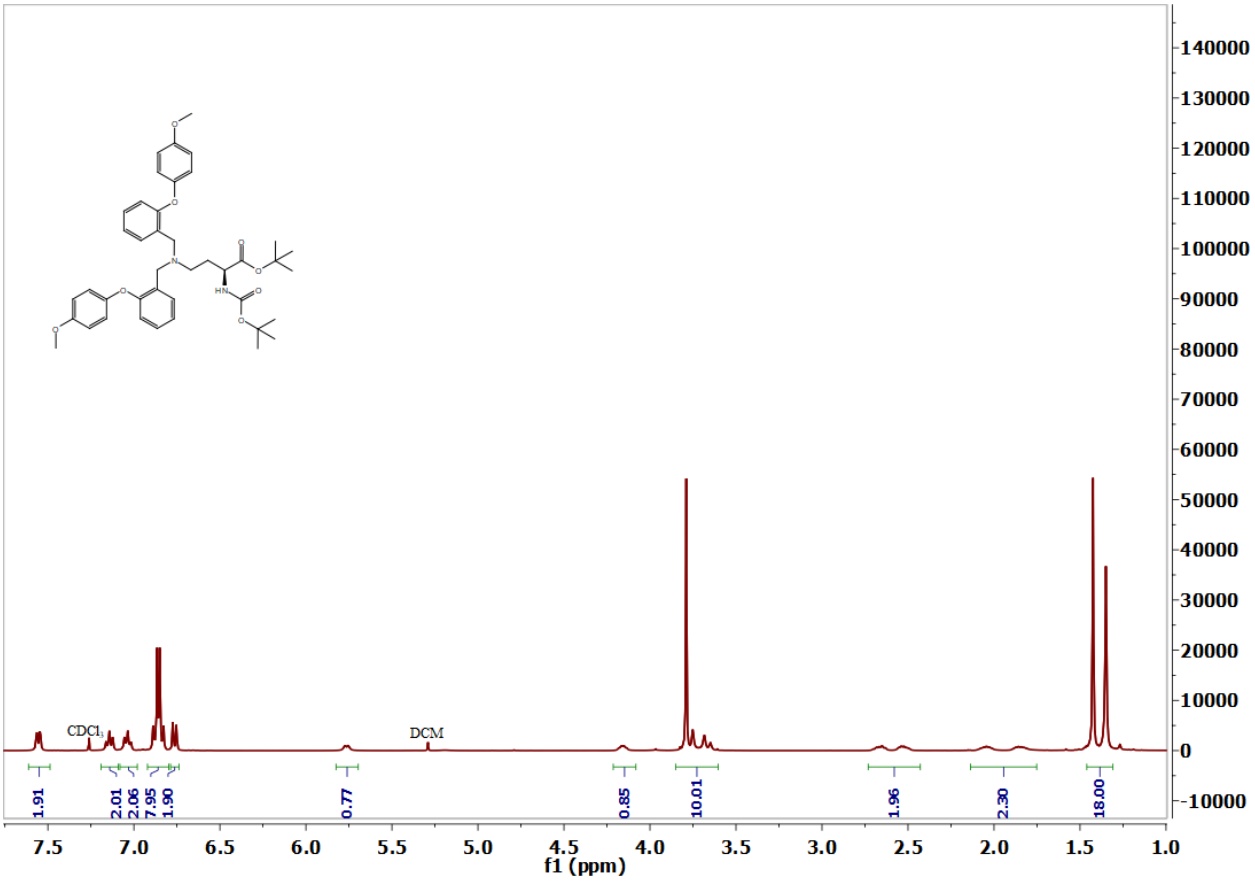

Figure 19: ^{1}H NMR (400 MHz, $CDCl_3$) δ 7.56 (d, J = 7.2 Hz, 1H), 7.14 (t, J = 7.1 Hz, 1H), 7.03 (dd, J = 9.6, 5.0 Hz, 1H), 6.90 – 6.81 (m, 4H), 6.76 (d, J = 8.0 Hz, 1H), 5.76 (d, J = 7.4 Hz, 1H), 4.16 (d, J = 4.6 Hz, 1H), 3.79 (s, 4H), 3.77 – 3.62 (m, 2H), 2.61 (ddd, J = 49.4, 12.7, 6.5 Hz, 1H), 2.12 – 1.75 (m, 1H), 1.42 (s, 5H), 1.35 (s, 5H).

3.2.2: Compound 12 Protected

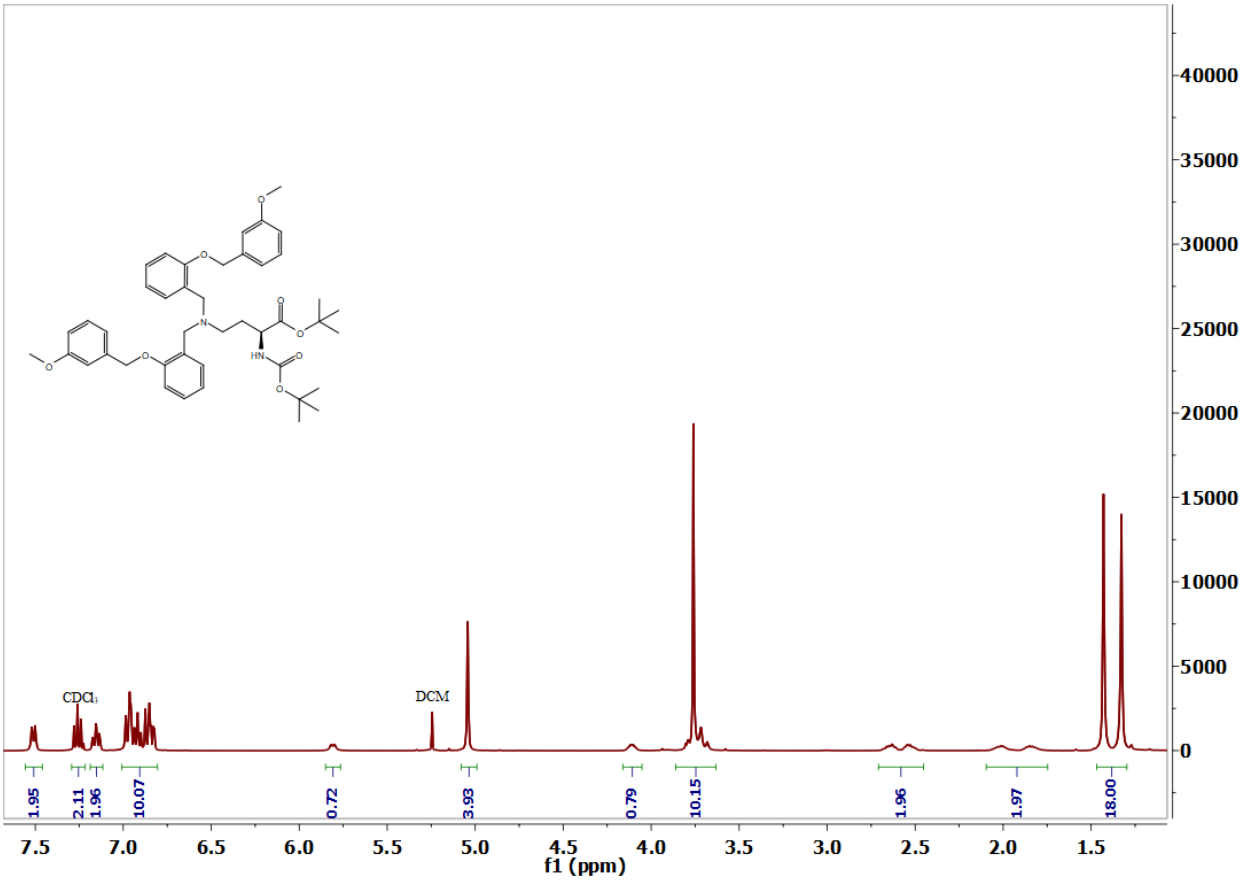

Figure 20: ^{1}H NMR (400 MHz, $CDCl_3$) δ 7.51 (d, J = 7.1 Hz, 2H), 7.25 (dd, J = 14.5, 6.7 Hz, 2H), 7.19 – 7.12 (m, 2H), 7.01 – 6.80 (m, 10H), 5.81 (d, J = 7.2 Hz, 1H), 5.04 (s, 4H), 4.11 (d, J = 4.9 Hz, 1H), 3.86 – 3.63 (m, 10H), 2.71 – 2.45 (m, 2H), 2.10 – 1.75 (m, 2H), 1.38 (d, J = 40.6 Hz, 18H).

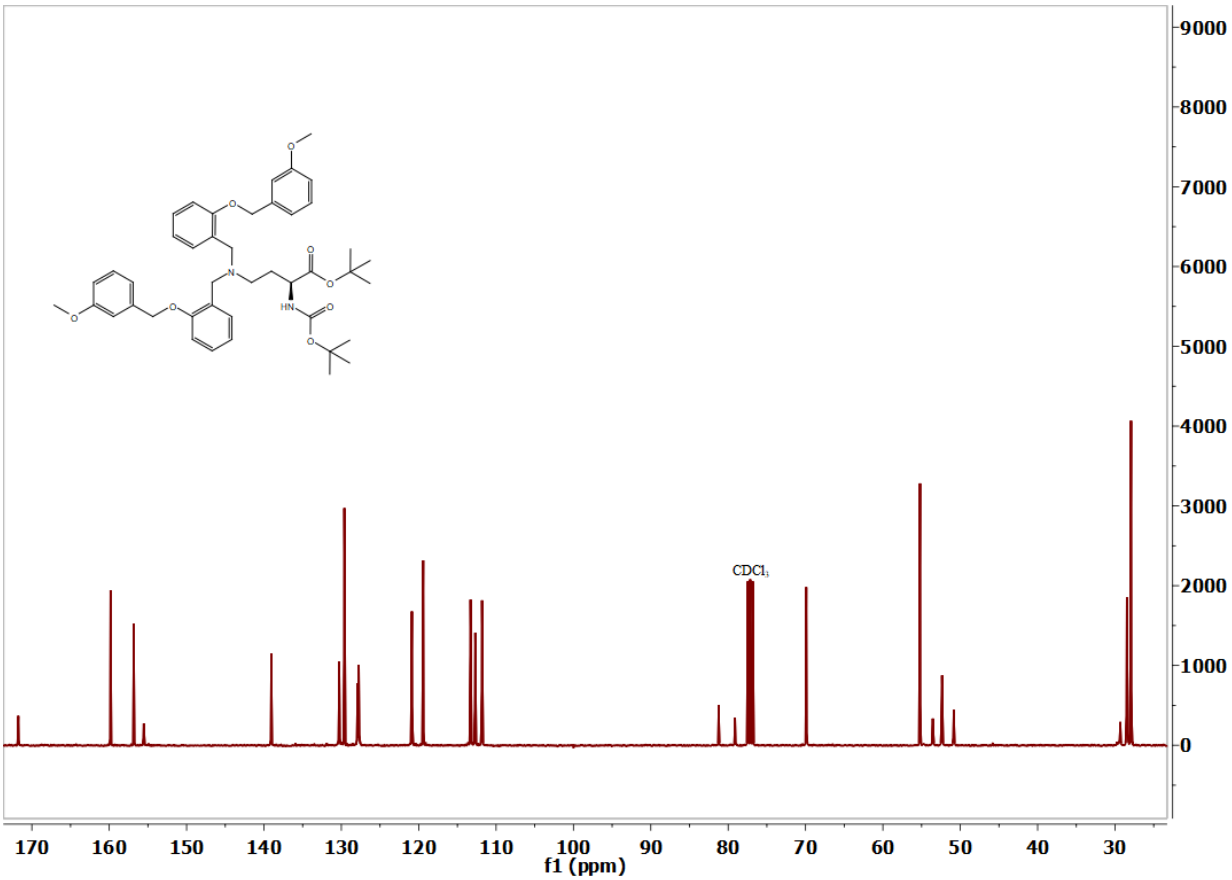

Figure 21: ^{13}C NMR (101 MHz, $CDCl_3$) δ 171.75 (s), 159.83 (s), 156.83 (s), 155.53 (s), 139.05 (s), 130.27 (s), 129.61 (s), 127.91 (s), 127.74 (s), 120.88 (s), 119.42 (s), 113.30 (s), 112.69 (s), 111.81 (s), 81.23 (s), 79.12 (s), 69.91 (s), 55.20 (s), 53.55 (s), 52.36 (s), 50.84 (s), 29.32 (s), 28.47 (s), 27.93 (s).

3.2.3: Compound 12 Deprotected

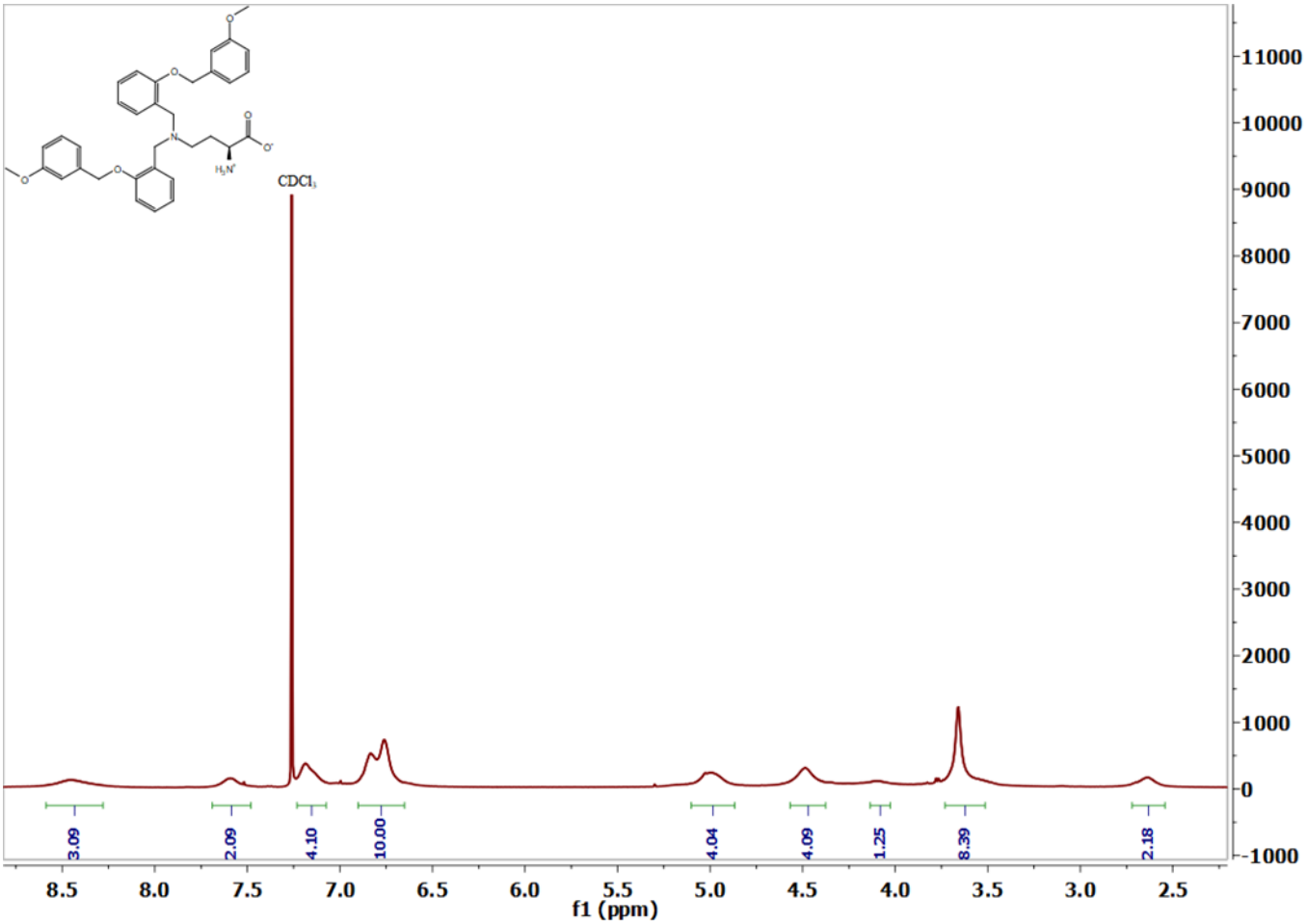

Figure 22: ^{1}H NMR (400 MHz, $CDCl_3$) δ 8.45 (s, 3H), 7.56 (d, J = 30.0 Hz, 2H), 7.19 (s, 4H), 6.80 (d, J = 29.6 Hz, 10H), 5.01 (d, J = 12.3 Hz, 4H), 4.49 (s, 4H), 4.10 (s, 1H), 3.66 (s, 8H), 2.63 (s, 2H).

3.2.4: Compound 19 Protected

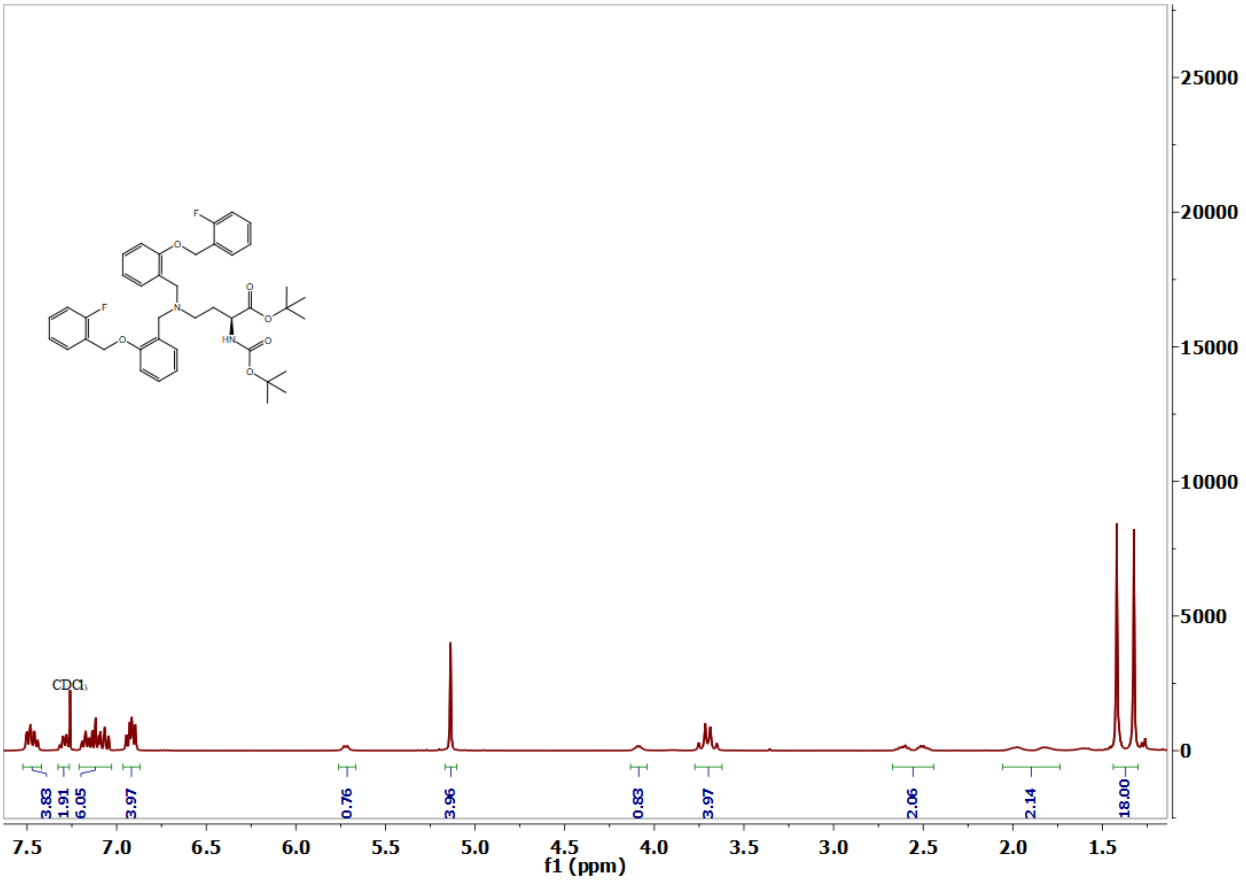

Figure 23: ^{1}H NMR (400 MHz, $CDCl_3$) δ 7.47 (dd, J = 16.3, 7.3 Hz, 4H), 7.33 – 7.26 (m, 2H), 7.21 – 7.03 (m, 6H), 6.92 (dd, J = 12.1, 7.8 Hz, 4H), 5.72 (d, J = 7.4 Hz, 1H), 5.14 (s, 4H), 4.09 (d, J = 5.1 Hz, 1H), 3.70 (q, J = 14.5 Hz, 4H), 2.67 – 2.44 (m, 2H), 2.06 – 1.74 (m, 2H), 1.44 – 1.30 (m, 18H).

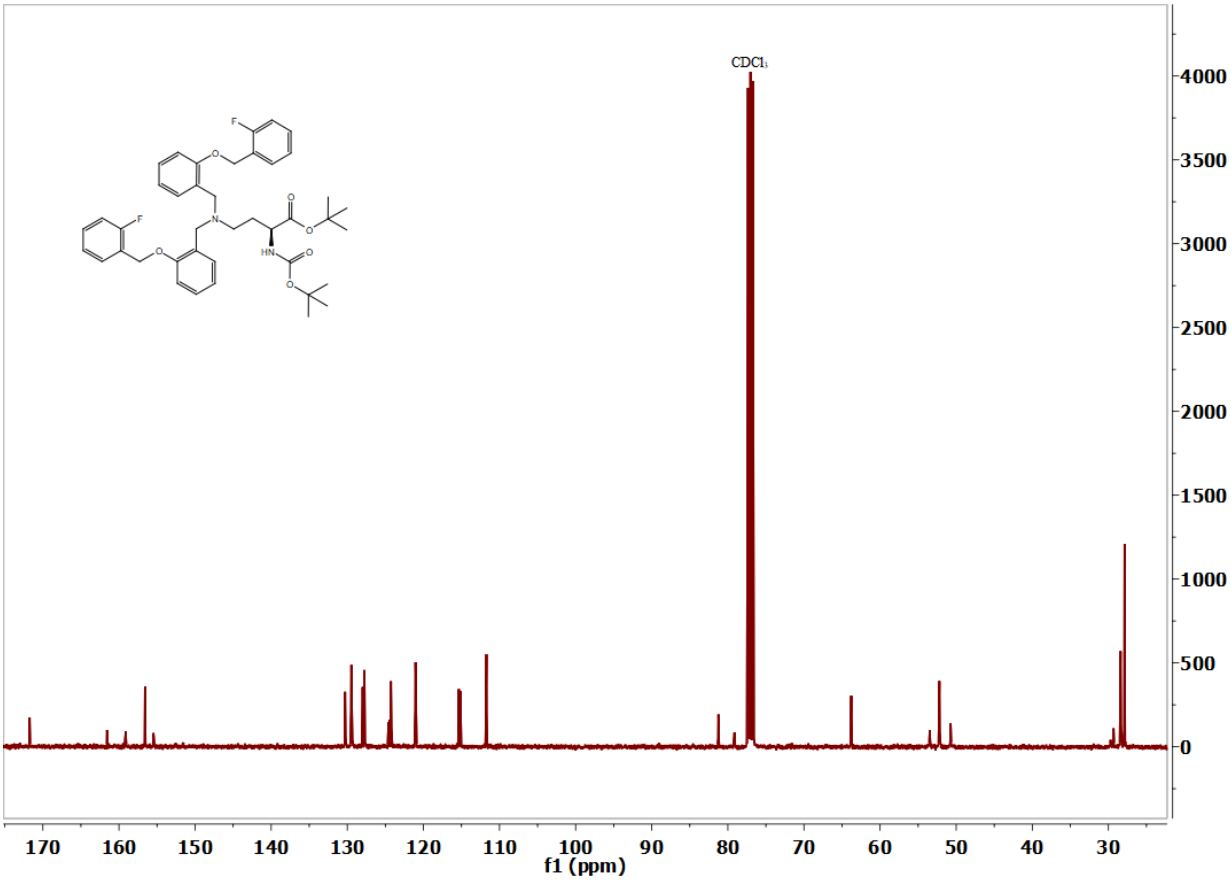

Figure 24: ^{13}C NMR (101 MHz, $CDCl_3$) δ 171.74 (s), 161.57 (s), 159.12 (s), 156.58 (s), 155.46 (s), 130.29 (s), 129.43 (d, J = 8.2 Hz), 127.98 (s), 127.75 (s), 124.60 (s), 124.46 (s), 124.24 (d, J = 3.5 Hz), 121.03 (s), 115.34 (s), 115.13 (s), 111.72 (s), 81.24 (s), 79.13 (s), 63.81 (d, J = 4.4 Hz), 53.48 (s), 52.21 (s), 50.73 (s), 29.31 (s), 28.40 (s), 27.88 (s).

3.2.5: Compound 19s: Protected

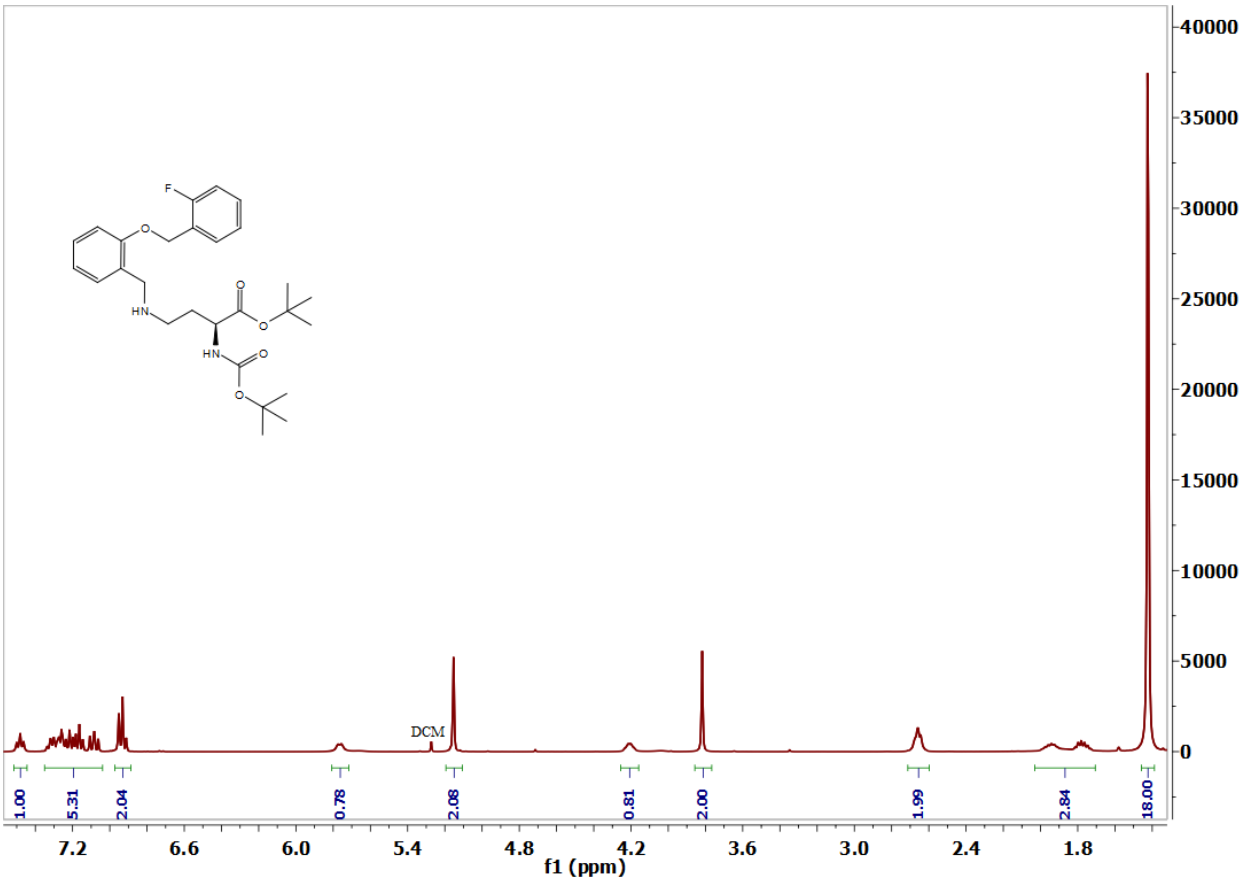

Figure 25: ^{1}H NMR (400 MHz, $CDCl_3$) δ 7.48 (t, J = 7.2 Hz, 1H), 7.35 – 7.04 (m, 5H), 6.93 (t, J = 8.0 Hz, 2H), 5.76 (d, J = 6.8 Hz, 1H), 5.15 (s, 2H), 4.21 (d, J = 4.7 Hz, 1H), 3.82 (s, 2H), 2.67 (dd, J = 16.3, 10.9 Hz, 2H), 2.03 – 1.71 (m, 3H), 1.42 (d, J = 2.1 Hz, 18H).

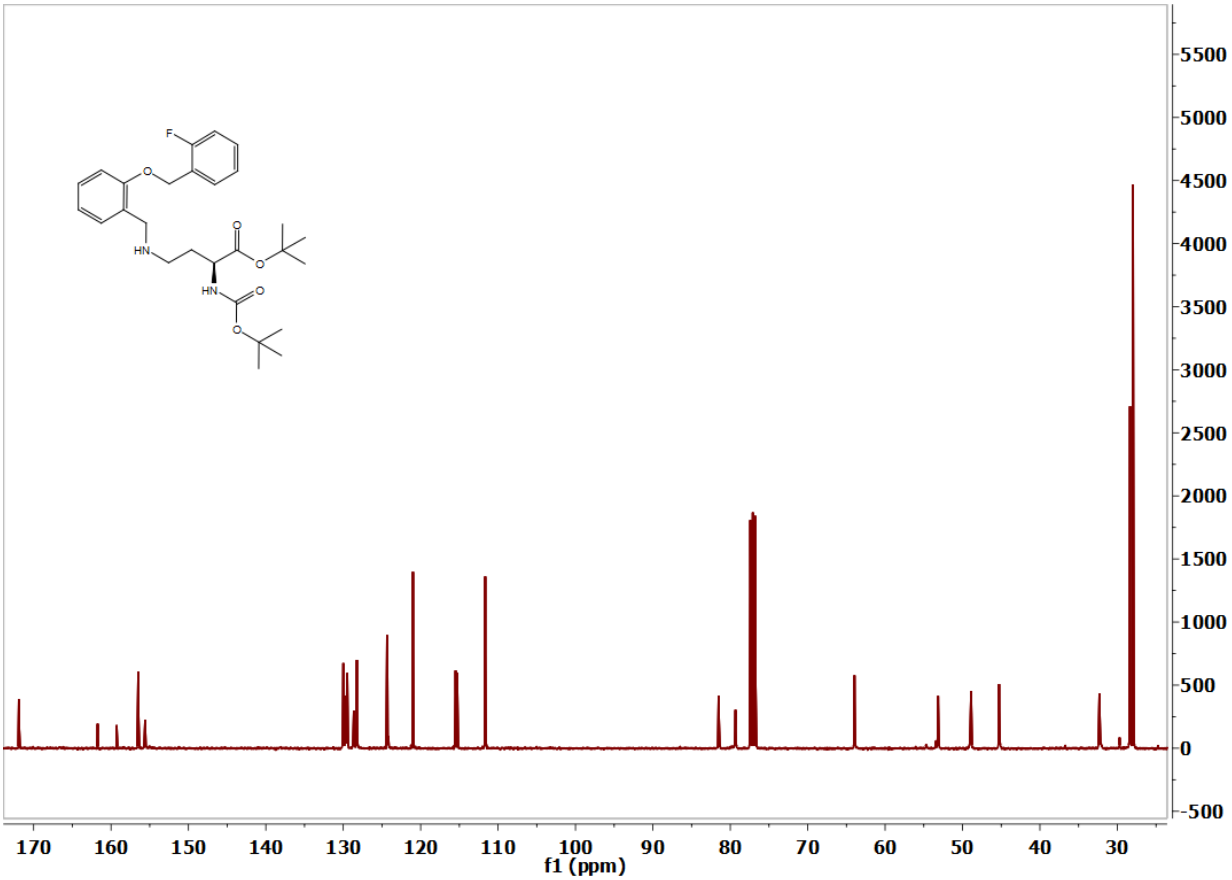

Figure 26: ^{13}C NMR (101 MHz, $CDCl_3$) δ 171.91 (s), 161.73 (s), 159.27 (s), 156.49 (s), 155.60 (s), 129.99 (s), 129.71 (d, J = 8.1 Hz), 129.50 (d, J = 4.0 Hz), 128.64 (s), 128.24 (s), 124.37 – 124.15 (m), 120.99 (s), 115.39 (d, J = 21.1 Hz), 111.66 (s), 81.51 (s), 79.33 (s), 63.93 (d, J = 4.3 Hz), 53.15 (s), 48.89 (s), 45.27 (s), 32.31 (s), 28.36 (s), 27.98 (s).

3.3: Patch Clamp Data: Dose Response Curves and Current Traces

Functional properties of the synthesized compounds were tested using whole-cell recording of voltage clamped HEK293 cells, which were transfected with the corresponding transporter DNA's. For non-competitive experiments of cells transfected with ASCT2, inwardly directed currents represent the 1 mM alanine control. The inward current is a result of increased leak anion conductance of SCN^- through ASCT2's anion conducting pore down its concentration gradient from the cytosol to the extracellular solution. Apparent outward currents for these experiments are the result of the application of a compound that inhibits the leak anion conductance. To generate a dose response curve for these experiments, the current relative to the current produced by the highest inhibitor concentration is plotted over increasing concentrations of inhibitor and fitted to a Michaelis-Menten like equation to obtain the K_i values found in Table 2. For competitive experiments conducted with either hASCT2 or rSNAT2, the decrease in the magnitude of the inwardly directed alanine current is measured with the application of increasing inhibitor concentrations and fit to a Michaelis-Menten like curve after plotting the value of these currents relative to the alanine control up to the highest inhibitor concentration used. The K_i values obtained for these "competition experiments" represent the K_i value of the compound at a concentration of 200 μM alanine.

3.3.1: Compound 6

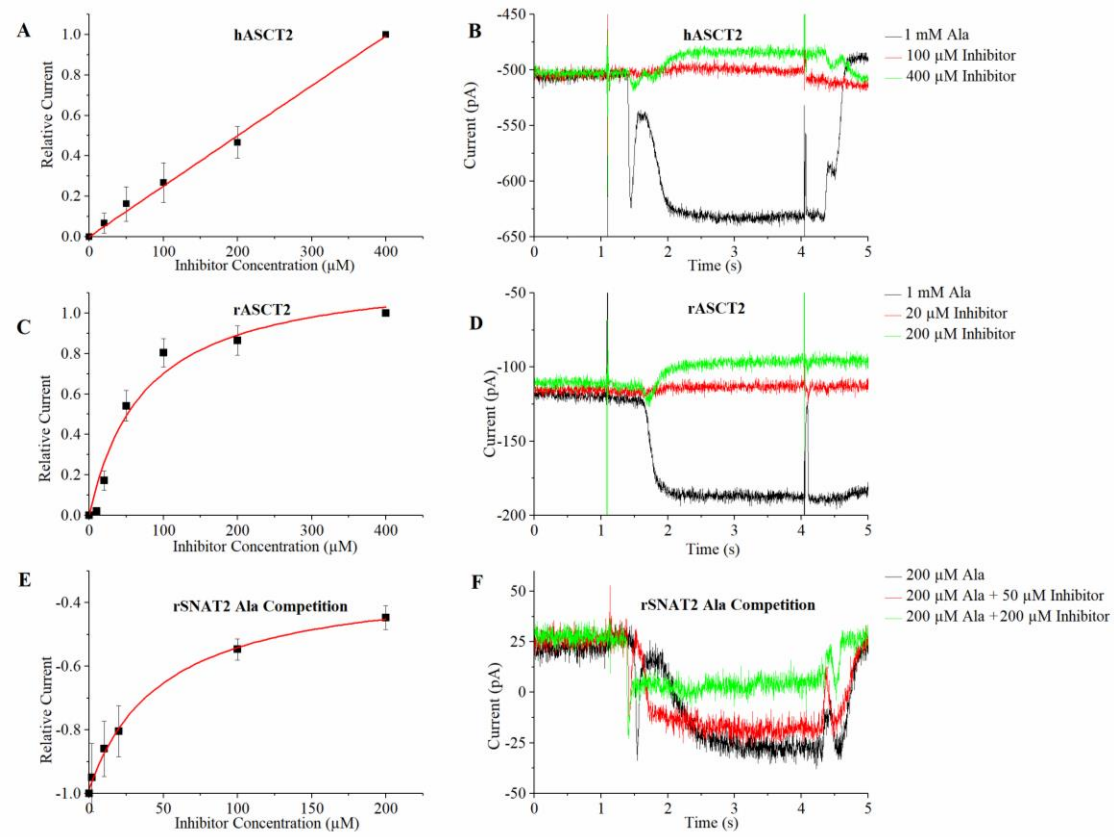

Figure 27: Compound 6 dose response curves and current recording traces for hASCT2 (A,B), rASCT2 (C,D), and rSNAT2 (E,F). SNAT2 experiments were done with increasing inhibitor concentrations in the presence of constant 200 μM Ala.

Compound 6 was one of the two compounds to show significant apparent outwardly directed currents in a dose dependent manner for hASCT2 and rASCT2, indicative of inhibitory behavior. However, while application of increasing concentrations of the compound to HEK293 cells expressing rASCT2 resulted in a dose response relationship that started saturating at high concentrations, currents elicited in hASCT2 increased with concentration in a linear fashion and not a hyperbolic curve. Therefore, no K_i could be determined for hASCT2 (Figs. 27A & B). From the dose response curve for rASCT2 (Figs. 27C & D) a K_i of 74.2 ± 23.4 μM was

determined. It should be noted that these values were obtained in the absence of transported substrate, alanine, and, thus, reflect intrinsic K_i values for ASCT2s.

For SNAT2, in contrast, no outward currents were observed in the absence of alanine, either in the presence or absence of SCN^-, indicating that compound 6 was unable to block leak anion current in this transporter. For this reason, compound 6 was applied in the presence of alanine, to test whether it was able to inhibit the alanine-induced transport current. As shown in Fig. 27F, compound 6 reduced inwardly directed alanine transport current in a dose dependent manner. While it was not possible to fully block transport current, given the limited accessible concentration range due to solubility problems at concentrations higher than 200 μM, a dose response curve of the blocking effect could be constructed (Fig. 27E). Analysis of the dose response relationship with equations found in Figure 6 resulted in a K_i of 50.4 ± 8.4 μM for rSNAT2. Clearly, these data show that compound 6 is a more potent inhibitor for SNAT2 than for ASCTs.

3.3.2: Compound 12

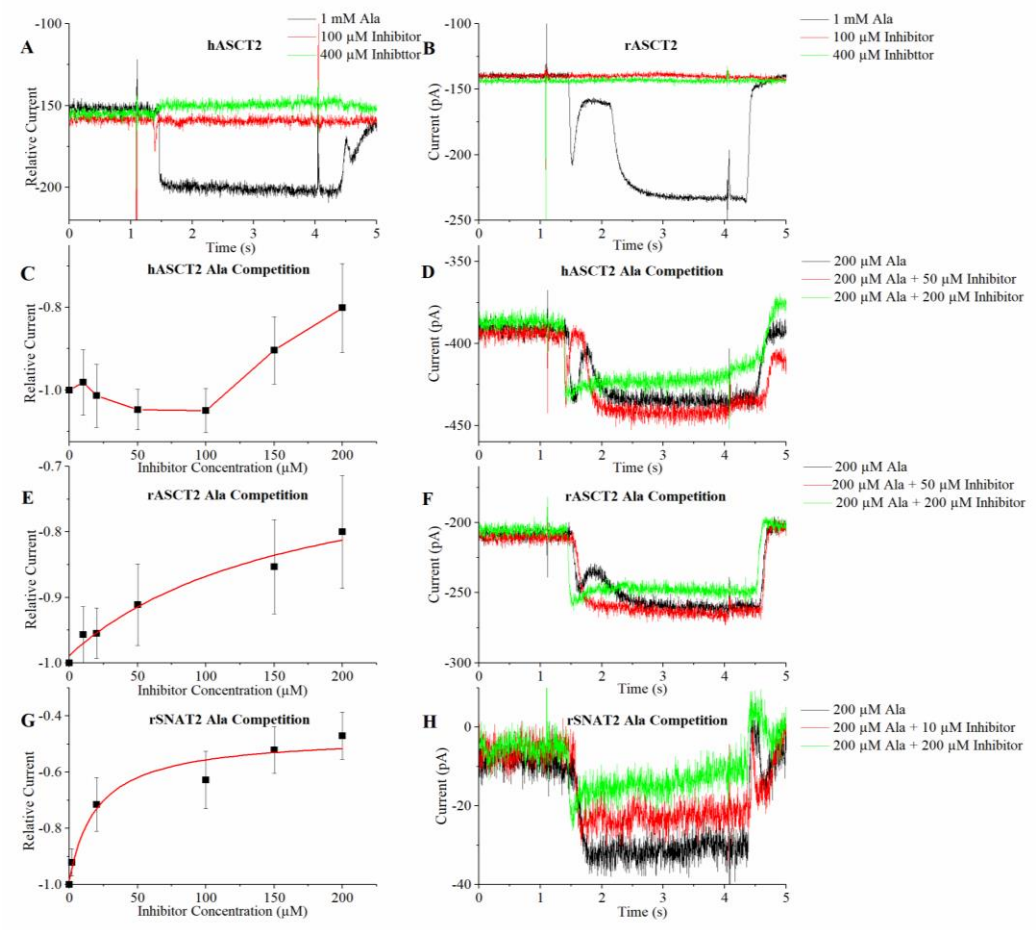

Figure 28: Compound 12 dose response curves and current recording traces for hASCT2 (A,C,D), rASCT2 (B,E,F), and rSNAT2 (G,H). All dose response curves were done under competitive inhibition experiments with 200 µM Ala.

Small apparent outwardly directed currents were produced in hASCT2 HEK293 cells by application of high concentrations (400 µM) of compound 12, but virtually no response was seen below concentrations of 400 µM in either hASCT2 or rASCT2 (Figs. 28A & B). For both hASCT2 and rASCT2 expressing HEK293 cells, competitive experiments with 200 µM alanine showed some inhibition at concentrations greater than 100 µM, however, the data for both could not be fit to obtain a K_i value for either transporter (Figs. 28C-28F). In SNAT2 expressing cells,

no outward or inward currents were produced in the absence of alanine, but in the presence of alanine, showed inhibition in a dose dependent manner and the data fit to a K_i value of 20.8 ± 12.3 μM (Fig. 28G). However, compound 12, like compound 6, could not completely block the alanine induced transport current (Fig. 28H). This is seen for every compound that is a SNAT2 inhibitor.

3.3.3: Compound 19

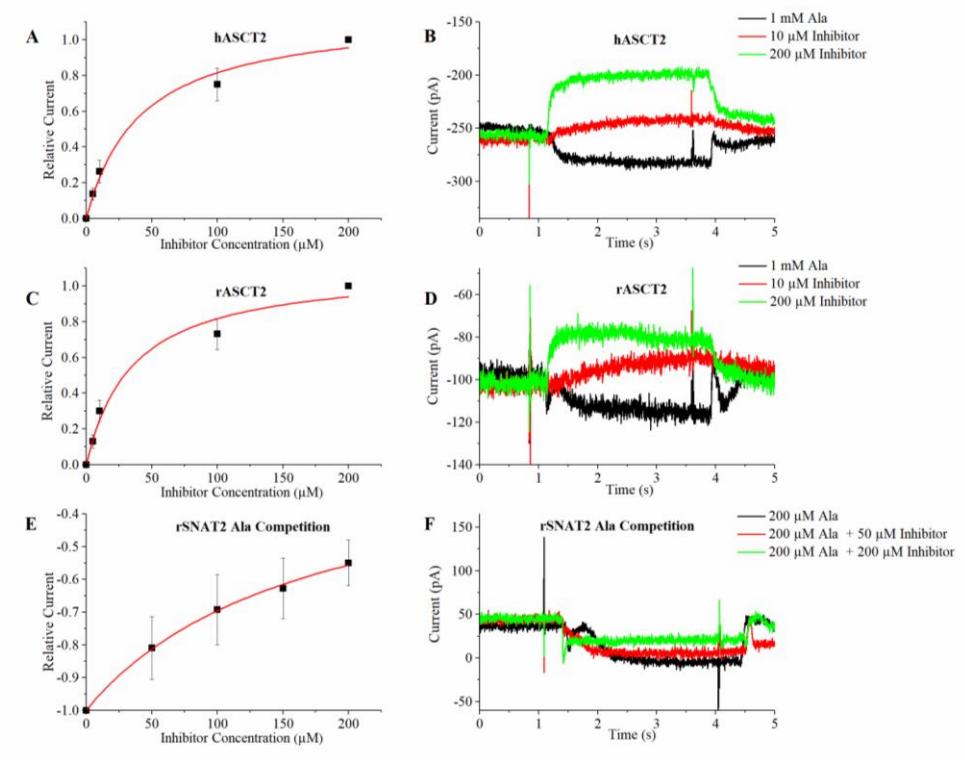

Figure 29: Compound 19 dose response curves and current recording traces for hASCT2 (A,B), rASCT2 (C,D), and rSNAT2 (E,F). SNAT2 experiments were done with increasing inhibitor concentrations in the presence of constant 200 μM Ala.

Compound 19 showed significant outward currents for both hASCT2 and rASCT2, which were concentration dependent with K_i values of 41.1 ± 12.3 μM and 34.9 ± 13.4 μM (Figs. 29A-29D). The K_i values obtained here indicate that compound 19 has the highest binding affinity to ASCT2 out of all the tested compounds. As for compound 6, compound 19 did not elicit currents

in rSNAT2-transfected cells in the absence of alanine. However, inhibition of alanine-induced transport currents was observed, but did not saturate at concentrations up to 200 μM (Fig. 29E) Inhibition of rSNAT2 by compound 19 had the lowest binding affinity for rSNAT2 out of all the tested compounds with a K_i value of 168.9 ± 32.1 μM (Fig. 29E & F).

3.3.4: Compound 19s

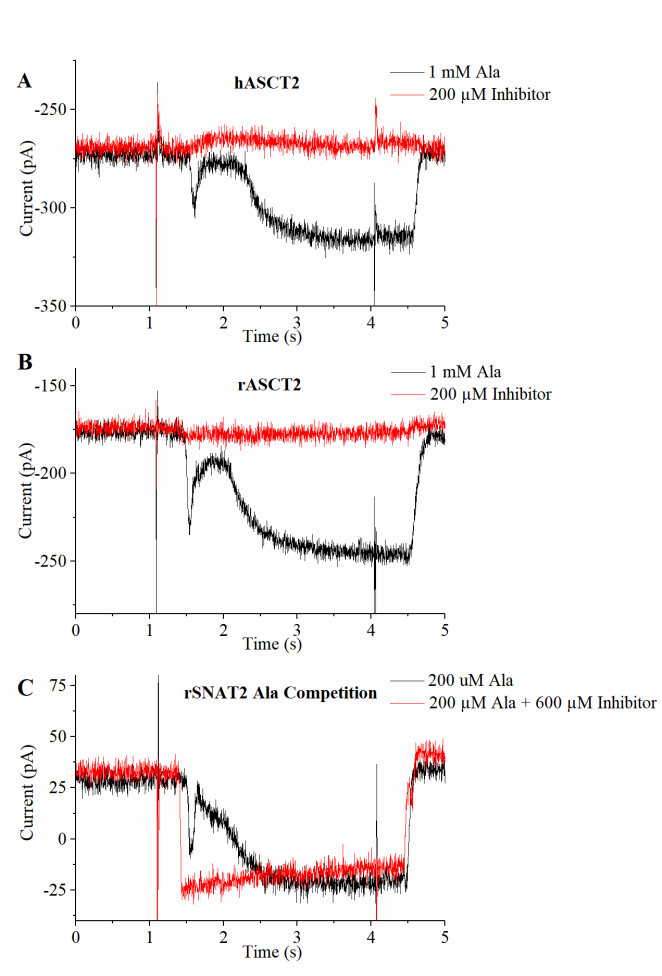

Figure 30: Compound 19s current traces for hASCT2 (A), rASCT2 (B), and rSNAT2 (C). Dose response curves were not plotted for this compound as there was little to no response for each protein with increasing applications of inhibitor.

The analogue of compound 19, 19s, with a single-coupled side chain showed little outward current at the highest concentration tested using hASCT2, 200 μM. Currents below 200

μM inhibitor showed no response (Fig. 30A). rASCT2 cells showed no response even at 200 μM inhibitor (Fig. 30B). These results indicate that compound 19s is not an inhibitor of ASCT2. Competitive inhibition experiments were not done for these two transporters. For rSNAT2, compound 19s was tested in the presence of alanine. At concentrations up to 600 μM, there was virtually no inhibition of the alanine-induced inward transport current (Fig. 30C). Together, these data suggest that compound 19s is ineffective as an inhibitor with respect to both ASCT2 and SNAT2.

3.3.5: V-9302

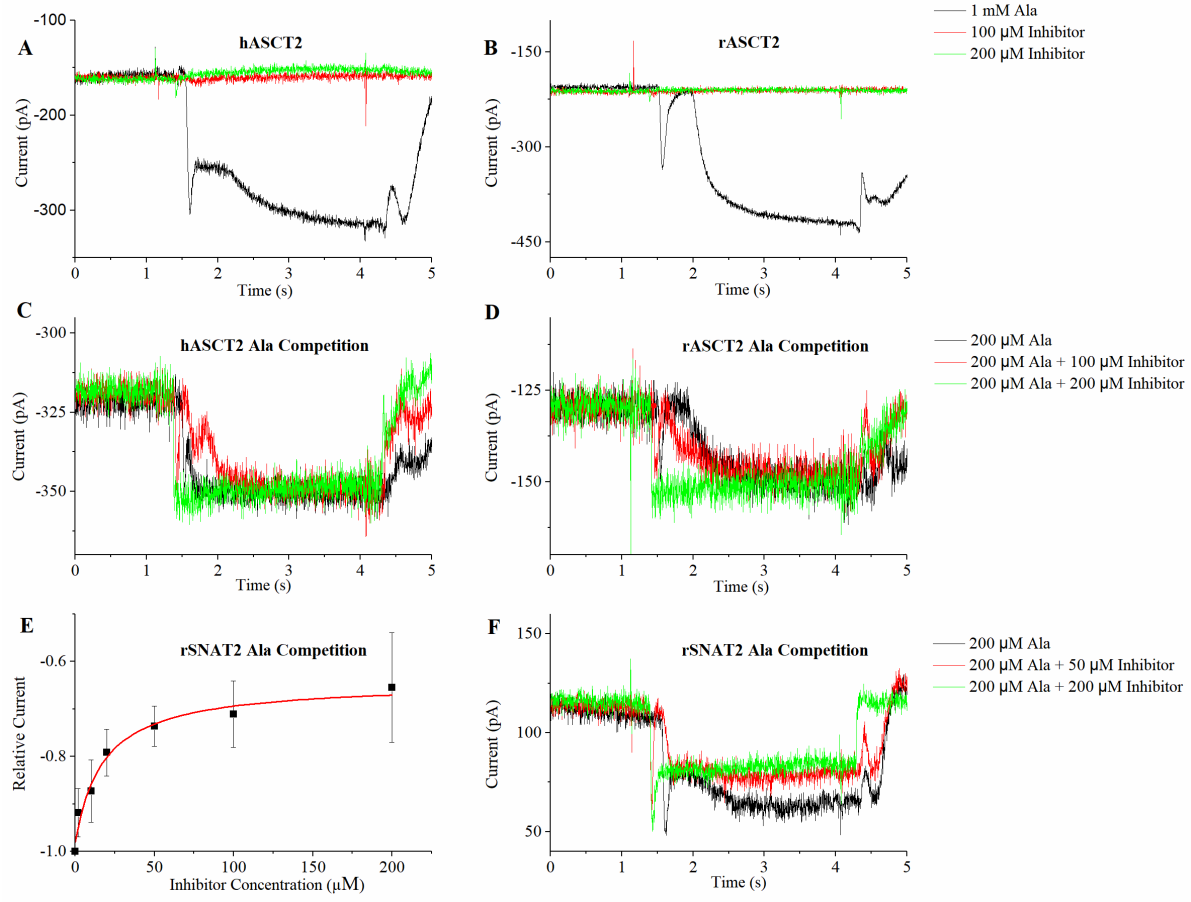

Figure 31: V-9302 dose response curves and current recording traces for hASCT2 (A,C), rASCT2 (B,D) and rSNAT2 (E,F). The key used for B is the same for A and the key for D is the same for C.

V-9302 is the only inhibitor from the aminobutyric acid derivatives published by Schulte et al. (2016 & 2018), that is commercially available. Therefore, this compound was not synthesized, but purchased from MedChem Express. V-9302 was reported to inhibit ASCT2 with low micromolar affinity (Schulte, M. et al., 2018). In contrast to these literature results, inhibitory function could not be detected in the work presented here. Very small apparently outward currents were visible for hASCT2 at 200 μM inhibitor but not for rASCT2 (Figs. 31A & B). At lower concentrations, current responses were too small to be analyzed (< 5 pA). To test for block of alanine-induced current, V-9302 was co-applied with 200 μM alanine (Figs. 31C & D). No inhibition of the alanine current was observed in the accessible concentration range. Therefore, dose response curves for competitive alanine experiments for hASCT2 and rASCT2 are not shown.

For rSNAT2, V-9302 inhibited alanine-induced inward transport current, although no complete block was observed at the highest concentration tested (Fig. 31F). After plotting the current vs. the V-9302 concentration, an apparent K_i value of 17.7 ± 5.5 μM was obtained (Fig. 31E). However, due to the block of alanine current of only 40% at maximum V-9302 concentration, it is not clear how reliable this K_i value is. Clearly, a competitive inhibition mechanism would require the compound to completely block alanine-induced transport current. This is not the case in the data presented here. Therefore, either the data are not of sufficient quality to determine K_i for competitive blocking, or the mechanism of inhibition is different from a competitive mechanism. Additional experiments will have to be performed to differentiate between these possibilities. Overall, each tested compound shows an inhibitory effect towards rSNAT2 by inhibiting the inward alanine substrate induced current. In addition, the data shows evidence that slight changes in structure in the side chains of the tested AABA compounds

significantly change the inhibitory character of these compounds toward the ASCTs and SNAT2. In addition, while the data for each SNAT2 experiment fit to a dose response curve to a K_i value, the tested compounds did not completely inhibit the alanine induced currents. Future experimentation with higher concentrations is difficult due to the poor solubility of most of these compounds at concentrations greater than 200 μM. Experiments in the future with lower alanine concentrations are a possibility to examine if the alanine induced current is inhibited completely by these compounds. The summary of the K_i values obtained for each compound for each respective transporter is illustrated in Table 2,

Table 2: K_i values obtained for each compound. All values marked with N/A indicate that a K_i value could not be calculated due to poor binding affinity of the compound to the respective transporter. All K_i values obtained for rSNAT2 were obtained in the presence of constant 200 μM Ala.

Compound	K_i (μM): hASCT2	K_i (μM): rASCT2	K_i (μM): rSNAT2
6	> 400	74.2 ± 23.4	50.4 ± 8.4
12	N/A	N/A	20.8 ± 12.3
19	41.1 ± 12.3	34.9 ± 13.4	168.9 ± 32.1
19s	N/A	N/A	N/A
V-9302	N/A	N/A	17.7 ± 5.5

Chapter 4: Discussion

The synthesis of small molecule inhibitors of ASCT2 is a widely growing area of research due to the upregulation of this protein in different cancers such as breast and prostate cancer (Wang, Q., et al., 2015; Van Geldermalsen, M., et al., 2016). Experiments using shRNA knockdown of ASCT2 *in vivo* and *in vitro* have shown significant decreases in tumor growth and metastasis, in addition to decreased tumor growth using chemical inhibition of ASCT2 (Wang, Q. et al., 2015). However, the lack of specific, potent ASCT2 inhibitors prevents the use of chemical inhibition of ASCT2 in clinical settings and the development of these inhibitors would be an invaluable tool in treating different cancers by glutamine starvation. While AABA inhibitors have been shown to slow tumor growth both *in vivo* and *in vitro*, the specificity of these compounds in the inhibition of glutamine uptake by ASCT2 has been contested in other studies (Schulte, M., et al. 2016 & 2018; Bröer, A., et al. 2018). Instead, it is suspected that these AABA inhibitors are not specific to ASCT2 at all, but rather SNAT2 and LAT1. However, these studies only picked two of the more potent inhibitors tested by Schulte et al. and did not characterize other compounds in the library of purported ASCT2 inhibitors (Bröer, A. et al., 2018). Additionally, no prior studies have characterized the binding affinity of these inhibitors using electrophysiological methods and reported accurate K_i values.

My electrophysiological characterization of these inhibitors on ASCT2 and SNAT2 shows evidence that these compounds are SNAT2 blockers. Some compounds, such as compound 6 and 19, have additional inhibitory effects on ASCT2 (Fig. 27 & 29), and the others, 12, 19s, and V-9302, show little to none (Fig. 28, 30, &31). The two AABA compounds tested by Bröer, A., et al., Compound 12 and V-9302, show the weakest response to both hASCT2 and rASCT2. In normal electrophysiological experiments, a small, apparent outward current is only

seen with 400 μM inhibitor for hASCT2, while there is no response from rASCT2 at the same concentration of inhibitor with compound 12 (Figure 28A & 28B). Competitive experiments with 200 μM alanine show a small amount of inhibition as compared to the control for both rASCT2 and hASCT2 (Figure 28 C-F), but not at the binding affinities reported in the literature. V-9302 shows a similar trend, with some current response at 200 μM for hASCT2, but no response for rASCT2 (Figure 31A & 31B). The data presented here contrast the results reported by Schulte et al. (2016 & 2018), who reported that compound 12 and V-9302 had high affinity interaction specifically to ASCT2. My electrophysiological characterization points to evidence that the clinical effects of these compounds are unlikely caused by block of ASCT2 because of the poor interaction with ASCT2. Instead, the clinical effects of decreased glutamine uptake are likely due to the inhibition of different amino acid transporters, such as SNAT2.

In addition, out of all the compounds tested, 12 and V-9302 potentially show the highest binding affinity to rSNAT2, with K_i values of 20.8 ± 12.3 μM and 17.7 ± 5.5 μM respectively (Table 2). V-9302, however, only shows a decrease of approximately 40% in a dose dependent manner and solubility issues prevent electrophysiological testing at concentrations greater than 200 μM. Therefore, it is not known how reliable the K_i value of V-9302 for SNAT2 is and there is a possibility that it could be higher or that inhibition occurs by a different mechanism than competitive inhibition. In addition, future experiments may be performed using lower concentrations of alanine to see if there is complete inhibition of the alanine induced current at lower concentrations. Importantly, these are the first non-transportable substrate blockers identified for SNAT2, which are not substrate-like inhibitors, such as α-(methylamino) isobutyric acid (MeAIB) (Yao, D. et al., 2000). This data shows increasingly supporting evidence that two of the most potent purported ASCT2 inhibitors actually have very poor binding affinity to

ASCT2 and instead rather act on SNAT2. However, two of the other compounds, 6 and 19, were weaker inhibitors of SNAT2 but showed inhibitory effects toward hASCT2 and rASCT2. Compound 19 demonstrated the best binding affinity to both hASCT2 and rASCT2 out of all the compounds tested with K_i values of 41.1 ± 12.3 μM for hASCT2 and 34.9 ± 13.4 μM for rASCT2 (Table 2). Interestingly, this compound had the lowest binding affinity to SNAT2 (Table 2). Overall, compound 6 showed a similar trend, but had slightly poorer binding affinity to rASCT2 than compound 19. In addition, compound 6 showed an interesting current response to hASCT2, in which saturation could not be reached, even at concentrations of 400 μM inhibitor (Figure 27A). These data show evidence that slight modifications in the side chains of the AABA compounds can significantly change the inhibitory characteristics of the compounds.

Previously reported inhibitors of ASCT2 such as GPNA and other studies of the binding site of the SLC1A family have provided a scaffold for the synthesis of ASCT2 inhibitors (Esslinger, C. S. et al., 2005; Corti, A. et al., 2019). Later work in this area has shown that increasing the hydrophobicity of the side chains on inhibitory compounds led to increased inhibitor binding affinity (Albers, T. et al, 2012; Singh, K. et al., 2017). For example, studies conducted by Singh et al. (2017) found that increasing the hydrophobicity of the side chains of single substituted benzylproline derivatives was correlated with an increase in apparent binding affinity. In fact, electrophysiological characterization revealed a potent biphenyl benzylproline inhibitor with a K_i value of 3 ± 2 μM (Singh, K. et al., 2017). A similar trend was noted for inhibitory serine derivatives in a study conducted by Albers et al. (2012), which concluded that inhibitors of ASCT2 preferentially bind to the outward open conformation of ASCT2, in contrast to substrates, which preferentially preferred the closed-loop, outward occluded conformation. Results from this study found that the increased binding affinity was associated with long

hydrophobic side chains with aromatic bulk. However, side chains that had too much aromatic bulk, such as naphthyl, did not inhibit strongly, suggesting that too much aromatic bulk may lead to poor inhibition (Albers, T. et al., 2012). ASCT2 homology models have shown that there are two hydrophobic pockets in ASCT2, pocket A and B (Colas, C. et al., 2015). The results from the study conducted by Singh, et al. (2017) indicated that these inhibitors likely occupy pocket B, with only a single hydrophobic side chain (Singh, K. et al., 2017). Schulte et al. (2016) performed similar docking experiments with AABA inhibitors and found similar interactions with a hydrophobic pocket of ASCT2, in addition to interactions with a hairpin loop that likely closes over the substrate binding site. This interaction could prevent closing of this loop and be a possible mechanism of inhibition (Schulte, M. et al., 2016). However, based on the results from my electrophysiological characterization, it is possible that the side chains for compound 12 and V-9302 are too bulky and have poor binding interaction with one of the hydrophobic binding pockets. Compound 6 may have better binding affinity due to the shorter chain length. In addition, the results from compound 19 indicate that the position of a substituent (fluoro) may significantly alter the binding affinity to ASCT2 at the given chain length, as V-9302 and compound 19 have an almost identical side chain length. Additionally, fluorine groups have been shown to increase the binding affinity of certain drugs by various interactions, including one with a peptide bond (Müller, K. et al., 2007). This may also explain the increased affinity for ASCT2 of compound 19. These results indicate that while bulky, hydrophobic, aromatic groups are characteristic of better binding affinity for ASCT2 inhibitors, it is likely that the side chain length is an important factor in determining this binding affinity and side chains that are too long will have weak to no apparent inhibitory binding affinity to ASCT2.

SNAT2 transports short chain aliphatic amino acids, with a preference for alanine. It is also a glutamine transporter (Yao, D. et al., 2000). SNAT2 is an isoform of system A activity, an important Na^+ dependent intracellular amino transport activity that occurs in many tissues throughout the human body. System A activity, unlike other amino acid transport systems such as the ASC's, also recognizes N-methylamino acids such as α-(methylamino)isobutyric acid (MeAIB). MeAIB, is a substrate like competitive inhibitor for SNAT2 and the other proteins associated with system A activity such as SNAT1 and SNAT4 (Yao, D. et al., 2000; Nishimura, T. et al., 2014). My electrophysiological characterization provides conclusive evidence that the tested AABA compounds are the first known, non-substrate like inhibitors of SNAT2. These results can be useful in further understanding the structure, mechanism, and binding interactions of SNAT2, as current structural data for SNAT2 is scarce. There is no crystal structure present for SNAT2 in the literature. However, some important structural and functional components of SNAT2 have been identified, including a difsulfide bridge, a conserved Na^+ binding site, and a leak anion conductance (Chen, C. et al., 2000; Zhang, Z., & Grewer, C., 2007; Zhang, Z. et al., 2009). In addition to this, SNAT2 and its membrane transport family (SLC38), have been reported to be a member of a superfamily of transporters for cations and organic substrates, notably the SLC5 and 6 family of proteins. Specifically, it was reported that the SLC5/6 family of proteins contain a similar structural fold to the SLC38 family (Zhang, Z. et al., 2009).

Compound 19s showed a small current response in hASCT2 at 200 μM inhibitor concentration, no inhibition of rASCT2, and no inhibition of rSNAT2 even at 600 μM inhibitor (Figure 30). Lack of inhibitory response in ASCT2 was expected due to the drastic change in structure of the inhibitor by removal of a single side chain. Based on our electrophysiological data, the low micromolar IC_{50} (high apparent affinities) values reported by Schulte et al. (2016 &

2018) for the library of AABA compounds may have been obtained from the combined inhibition of glutamine uptake by the inhibition of both SNAT2 and ASCT2, while some compounds may have only inhibited SNAT2. In addition, there is evidence that compound 12 and V-9302 also display inhibitory effects towards another protein, LAT1 (Bröer, A. et al., 2018). However, electrophysiological current recordings are not useful in the determination of K_i values for inhibitors specific to LAT1 because of its electroneutral characteristics, so it would be difficult to confirm this by our electrophysiological methods (Scalise, M. et al., 2018).

Chapter 5: Conclusion

In conclusion, electrophysiological data presented here shows evidence that AABA compounds are more likely to be to SNAT2 inhibitors, rather than ASCT2 inhibitors. These compounds, specifically compound 12 and V-9302, can be used to further understand the binding site of SNAT2 and help in the development of pharmacophore models that allow the quantification of structure-junction parameters of amino acid derivative interaction with the binding site. However, the relatively high binding affinity of compound 19 opens a door for further exploration into these AABA inhibitors specifically for ASCT2. As indicated by the results, slight modifications to the side chains show significant changes to the binding affinity of these inhibitors towards ASCT2. There was a total of 23 characterized AABA inhibitors in the study done by Schulte et al. (2016) and further electrophysiological characterization of these compounds is necessary to find those with potentially higher binding affinities for ASCT2. While these compounds can no longer be reported as specific ASCT2 inhibitors, they are potentially useful in further understanding of the binding site for both ASCT2 and SNAT2.

Bibliography

Abdel-Magid, A. F., & Mehrman, S. J. (2006). A review on the use of sodium triacetoxyborohydride in the reductive amination of ketones and aldehydes. In *Organic Process Research and Development* (Vol. 10, Issue 5, pp. 971–1031). American Chemical Society . https://doi.org/10.1021/op0601013

Albers, T., Marsiglia, W., Thomas, T., Gameiro, A., & Grewer, C. (2012). Defining substrate and blocker activity of alanine-serine- cysteine transporter 2 (ASCT2) ligands with novel serine analogs. *Molecular Pharmacology*, *81*(3), 356–365. https://doi.org/10.1124/mol.111.075648

Bröer, A., Fairweather, S., & Bröer, S. (2018). Disruption of Amino Acid Homeostasis by Novel ASCT2 Inhibitors Involves Multiple Targets. *Frontiers in Pharmacology*, *9*(JUL), 785. https://doi.org/10.3389/fphar.2018.00785

Bröer, A., Rahimi, F., & Bröer, S. (2016). Deletion of amino acid transporter ASCT2 (SLC1A5) Reveals an essential role for transporters SNAT1 (SLC38A1) and SNAT2 (SLC38A2) to sustain glutaminolysis in cancer cells. *Journal of Biological Chemistry*, *291*(25), 13194–13205. https://doi.org/10.1074/jbc.M115.700534

Bröer, A., Wagner, C., Lang, F., & Bröer, S. (2000). Neutral amino acid transporter ASCT2 displays substrate-induced Na^+ exchange and a substrate-gated anion conductance. Biochemical Journal, 346(3), 705–710. https://doi.org/10.1042/0264-6021:3460705

Bröer, S. (2014). The SLC38 family of sodium-amino acid co-transporters. In *Pflugers Archiv European Journal of Physiology* (Vol. 466, Issue 1, pp. 155–172). Springer. https://doi.org/10.1007/s00424-013-1393-y

Burlingham, B. T., & Widlanski, T. S. (2003). An intuitive look at the relationship of K_i and IC_{50}: A more general use for the dixon plot. *Journal of Chemical Education*, *80*(2), 214–218. https://doi.org/10.1021/ed080p214

Chen, C., Wang, J., Cai, R., Yuan, Y., Guo, Z., Grewer, C., & Zhang, Z. (2016). Identification of a Disulfide Bridge in Sodium-Coupled Neutral Amino Acid Transporter 2(SNAT2) by Chemical Modification. *PLOS ONE*, *11*(6), e0158319. https://doi.org/10.1371/journal.pone.0158319

Colas, C., Grewer, C., Otte, N. J., Gameiro, A., Albers, T., Singh, K., Shere, H., Bonomi, M., Holst, J., & Schlessinger, A. (2015). Ligand Discovery for the Alanine-Serine-Cysteine Transporter (ASCT2, SLC1A5) from Homology Modeling and Virtual Screening. *PLoS Computational Biology*, *11*(10). https://doi.org/10.1371/journal.pcbi.1004477

Corti, A., Dominici, S., Piaggi, S., Belcastro, E., Chiu, M., Taurino, G., Pacini, S., Bussolati, O., & Pompella, A. (2019). γ-Glutamyltransferase enzyme activity of cancer cells modulates L-γ-glutamyl-p-nitroanilide (GPNA) cytotoxicity. Scientific Reports, 9(1), 1–13. https://doi.org/10.1038/s41598-018-37385-x

Divito, C. B., & Underhill, S. M. (2014). Excitatory amino acid transporters: Roles in glutamatergic neurotransmission. In *Neurochemistry International* (Vol. 73, Issue 1, pp. 172–180). Elsevier Ltd. https://doi.org/10.1016/j.neuint.2013.12.008

Esslinger, C. S., Cybulski, K. A., & Rhoderick, J. F. (2005). Nγ-Aryl glutamine analogues as probes of the ASCT2 neutral amino acid transporter binding site. Bioorganic and Medicinal Chemistry, 13(4), 1111–1118. https://doi.org/10.1016/j.bmc.2004.11.028

Franchi-Gazzola, R., Gaccioli, F., Bevilacqua, E., Visigalli, R., Dall'Asta, V., Sala, R., Varoqui, H., Erickson, J. D., Gazzola, G. C., & Bussolati, O. (2004). The synthesis of SNAT2 transporters is required for the hypertonic stimulation of system A transport activity. *Biochimica et Biophysica Acta - Biomembranes*, *1667*(2), 157–166. https://doi.org/10.1016/j.bbamem.2004.09.012

Garaeva, A. A., Guskov, A., Slotboom, D. J., & Paulino, C. (2019). A one-gate elevator mechanism for the human neutral amino acid transporter ASCT2. *Nature Communications*, *10*(1), 1–8. https://doi.org/10.1038/s41467-019-11363-x

Goedhart, J., van Weeren, L., Adjobo-Hermans, M. J. W., Elzenaar, I., Hink, M. A., & Gadella, T. W. J. (2011). Quantitative Co-expression of proteins at the single cell level - application to a multimeric FRET sensor. *PLoS ONE*, *6*(11). https://doi.org/10.1371/journal.pone.0027321

Grewer, C., & Grabsch, E. (2004). New inhibitors for the neutral amino acid transporter ASCT2 reveal its Na+ -dependent anion leak. *Journal of Physiology*, *557*(3), 747–759. https://doi.org/10.1113/jphysiol.2004.062521

Grewer, C., Gameiro, A., Mager, T., & Fendler, K. (2013). Electrophysiological Characterization of Membrane Transport Proteins. *Annual Review of Biophysics*, *42*(1), 95–120. https://doi.org/10.1146/annurev-biophys-083012-130312

Hensley, C. T., Wasti, A. T., & DeBerardinis, R. J. (2013). Glutamine and cancer: Cell biology, physiology, and clinical opportunities. In Journal of Clinical Investigation (Vol. 123, Issue 9, pp. 3678–3684). American Society for Clinical Investigation. https://doi.org/10.1172/JCI69600

Hoffmann, T. M., Cwiklinski, E., Shah, D. S., Stretton, C., Hyde, R., Taylor, P. M., & Hundal, H. S. (2018). Effects of sodium and amino acid substrate availability upon the expression and stability of the SNAT2 (SLC38A2) amino acid transporter. *Frontiers in Pharmacology*, *9*(FEB), 63. https://doi.org/10.3389/fphar.2018.00063

Ji, Y., Postis, V. L. G., Wang, Y., Bartlam, M., & Goldman, A. (2016). Transport mechanism of a glutamate transporter homologue GltPh. *Biochemical Society Transactions*, *44*(3), 898–904. https://doi.org/10.1042/BST20160055

Jin, L., Alesi, G. N., & Kang, S. (2016). Glutaminolysis as a target for cancer therapy. In *Oncogene* (Vol. 35, Issue 28, pp. 3619–3625). Nature Publishing Group. https://doi.org/10.1038/onc.2015.447

Kanai, Y., & Hediger, M. A. (2004). The glutamate/neutral amino acid transporter family SLC1: Molecular, physiological and pharmacological aspects. In Pflugers Archiv European Journal of Physiology (Vol. 447, Issue 5, pp. 469–479). Springer. https://doi.org/10.1007/s00424-003-1146-4

Liberti, M. V, & Locasale, J. W. (2016). The Warburg Effect: How Does it Benefit Cancer Cells? HHS Public Access. *Trends Biochem Sci*, *41*(3), 211–218. https://doi.org/10.1016/j.tibs.2015.12.001

Molecular Devices (2012). *The Axon ™ Guide A guide to Electrophysiology and Biophysics Laboratory Techniques The Axon Guide to Electrophysiology and Biophysics Laboratory Techniques*. www.MolecularDevices.com

Müller, K., Faeh, C., & Diederich, F. (2007). Fluorine in pharmaceuticals: Looking beyond intuition. In *Science* (Vol. 317, Issue 5846, pp. 1881–1886). Science. https://doi.org/10.1126/science.1131943

Napoli, E., Bode, B. P., Scalise, M., Pochini, L., Console, L., Losso, M. A., & Indiveri, C. (2018). The Human SLC1A5 (ASCT2) Amino Acid Transporter: From Function to Structure and Role in Cell Biology. *Frontiers in Cell and Developmental Biology | Www.Frontiersin.Org*, *1*, 96. https://doi.org/10.3389/fcell.2018.00096

Ndaru, E., Garibsingh, R. A. A., Shi, Y. Y., Wallace, E., Zakrepine, P., Wang, J., Schlessinger, A., & Grewer, C. (2019). Novel alanine serine cysteine transporter 2 (ASCT2) inhibitors based on sulfonamide and sulfonic acid ester scaffolds. *Journal of General Physiology*, *151*(3), 357–368. https://doi.org/10.1085/jgp.201812276

Nishimura, T., Yagi, R., Usuda, M., Oda, K., Yamazaki, M., Suda, S., Takahashi, Y., Okazaki, F., Sai, Y., Higuchi, K., Maruyama, T., Tomi, M., & Nakashima, E. (2014). System A amino acid transporter SNAT2 shows subtype-specific affinity for betaine and hyperosmotic inducibility in placental trophoblasts. *Biochimica et Biophysica Acta - Biomembranes*, *1838*(5), 1306–1312. https://doi.org/10.1016/j.bbamem.2014.01.004

Palii, S. S., Chen, H., & Kilberg, M. S. (2004). Transcriptional Control of the Human Sodium-coupled Neutral Amino Acid Transporter System A Gene by Amino Acid Availability Is Mediated by an Intronic Element. *Journal of Biological Chemistry*, *279*(5), 3463–3471. https://doi.org/10.1074/jbc.M310483200

Scalise, M., Galluccio, M., Console, L., Pochini, L., & Indiveri, C. (2018). The human SLC7A5 (LAT1): The intriguing histidine/large neutral amino acid transporter and its relevance to human health. In *Frontiers in Chemistry* (Vol. 6, Issue JUN, p. 243). Frontiers Media S.A. https://doi.org/10.3389/fchem.2018.00243

Scopelliti, A. J., Font, J., Vandenberg, R. J., Boudker, O., & Ryan, R. M. (2018). Structural characterisation reveals insights into substrate recognition by the glutamine transporter ASCT2/SLC1A5. Nature Communications, 9(1), 1–12. https://doi.org/10.1038/s41467-017-02444-w

Schulte, M. L., Fu, A., Zhao, P., Li, J., Geng, L., Smith, S. T., Kondo, J., Coffey, R. J., Johnson, M. O., Rathmell, J. C., Sharick, J. T., Skala, M. C., Smith, J. A., Berlin, J., Kay Washington, M., Nickels, M. L., & Charles Manning, H. (2018). Pharmacological blockade of ASCT2-dependent glutamine transport leads to antitumor efficacy in preclinical models. *Nature Medicine*, *24*(2), 194–202. https://doi.org/10.1038/nm.4464

Schulte, M. L., Khodadadi, A. B., Cuthbertson, M. L., Smith, J. A., & Manning, H. C. (2016). 2-Amino-4-bis(aryloxybenzyl)aminobutanoic acids: A novel scaffold for inhibition of ASCT2-mediated glutamine transport Dedicated to the memory of Eric S. Dawson, Ph.D. *Bioorganic and Medicinal Chemistry Letters*, *26*(3), 1044–1047. https://doi.org/10.1016/j.bmcl.2015.12.031

Singh, K., Tanui, R., Gameiro, A., Eisenberg, G., Colas, C., Schlessinger, A., & Grewer, C. (2017). Structure activity relationships of benzylproline-derived inhibitors of the glutamine transporter ASCT2 HHS Public Access. *Bioorg Med Chem Lett*, *27*(3), 398–402. https://doi.org/10.1016/j.bmcl.2016.12.063

Souba, W. W. (1993). Glutamine and Cancer. In ANNALS OF SURGERY (Vol. 218, Issue 6).

Utsunomiya-Tate, N., Endou, H., & Kanai, Y. (1996). Cloning and functional characterization of a system ASC-like Na+-dependent neutral amino acid transporter. Journal of Biological Chemistry, 271(25), 14883–14890. https://doi.org/10.1074/jbc.271.25.14883

Van Geldermalsen, M., Wang, Q., Nagarajah, R., Marshall, A. D., Thoeng, A., Gao, D., Ritchie, W., Feng, Y., Bailey, C. G., Deng, N., Harvey, K., Beith, J. M., Selinger, C. I., O'Toole, S. A., Rasko, J. E. J., & Holst, J. (2016). ASCT2/SLC1A5 controls glutamine uptake and tumour growth in triple-negative basal-like breast cancer. *Oncogene*, *35*(24), 3201–3208. https://doi.org/10.1038/onc.2015.381

Wang, Q., Hardie, R. A., Hoy, A. J., Van Geldermalsen, M., Gao, D., Fazli, L., Sadowski, M. C., Balaban, S., Schreuder, M., Nagarajah, R., Wong, J. J. L., Metierre, C., Pinello, N., Otte, N. J., Lehman, M. L., Gleave, M., Nelson, C. C., Bailey, C. G., Ritchie, W., Holst, J. (2015). Targeting ASCT2-mediated glutamine uptake blocks prostate cancer growth and tumour development. *Journal of Pathology*, *236*(3), 278–289. https://doi.org/10.1002/path.4518

Yang, L., Venneti, S., & Nagrath, D. (2017). Glutaminolysis: A Hallmark of Cancer Metabolism. *Annual Review of Biomedical Engineering*, *19*(1), 163–194. https://doi.org/10.1146/annurev-bioeng-071516-044546

Yao, D., Mackenzie, B., Ming, H., Lè Ne Varoqui, H., Zhu, H., Hediger, M. A., & Erickson, J. D. (2000). *A Novel System A Isoform Mediating Na /Neutral Amino Acid Cotransport**. https://doi.org/10.1074/jbc.M002965200

Yu, X., Plotnikova, O., Bonin, P. D., Subashi, T. A., McLellan, T. J., Dumlao, D., Che, Y., Dong, Y. Y., Carpenter, E. P., West, G. M., Qiu, X., Culp, J. S., & Han, S. (2019). Cryo-EM structures of the human glutamine transporter SLC1a5 (ASCT2) in the outward-facing conformation. *ELife*, *8*. https://doi.org/10.7554/eLife.48120

Zhang, Z., Albers, T., Fiumera, H. L., Gameiro, A., & Grewer, C. (2009). A conserved Na^+ binding site of the sodium-coupled neutral amino acid transporter 2 (SNAT2). *Journal of Biological Chemistry*, *284*(37), 25314–25323. https://doi.org/10.1074/jbc.M109.038422

Zhang, Z., & Grewer, C. (2007). The sodium-coupled neutral amino acid transporter SNAT2 mediates an anion leak conductance that is differentially inhibited by transported substrates. *Biophysical Journal*, *92*(7), 2621–2632. https://doi.org/10.1529/biophysj.106.100776

Zhang, Z., Zander, C. B., & Grewer, C. (2011). The C-terminal domain of the neutral amino acid transporter SNAT2 regulates transport activity through voltage-dependent processes. *Biochemical Journal*, *434*(2), 287–296. https://doi.org/10.1042/BJ20100507